A natural product inhibits the initiation of α-synuclein aggregation and suppresses its toxicity

Michele Perni[a,b], Céline Galvagnion[a,1], Alexander Maltsev[c], Georg Meisl[a], Martin B. D. Müller[a,b], Pavan K. Challa[a], Julius B. Kirkegaard[d], Patrick Flagmeier[a], Samuel I. A. Cohen[a], Roberta Cascella[e], Serene W. Chen[a], Ryan Limboker[a], Pietro Sormanni[a], Gabriella T. Heller[a], Francesco A. Aprile[a], Nunilo Cremades[f], Cristina Cecchi[e], Fabrizio Chiti[e], Ellen A. A. Nollen[b], Tuomas P. J. Knowles[a], Michele Vendruscolo[a,2], Adriaan Bax[c,2], Michael Zasloff[g,2], and Christopher M. Dobson[a,2]

[a]Department of Chemistry, University of Cambridge, Cambridge CB2 1EW, United Kingdom; [b]University Medical Centre Groningen, European Research Institute for the Biology of Aging, University of Groningen, Groningen 9713 AV, The Netherlands; [c]Laboratory of Chemical Physics, National Institute of Diabetes and Digestive and Kidney Diseases, National Institutes of Health, Bethesda, MD 20892; [d]Department of Applied Mathematics and Theoretical Physics, University of Cambridge, Cambridge CB3 0WA, United Kingdom; [e]Department of Experimental and Clinical Biomedical Sciences, University of Florence, Florence 50134, Italy; [f]Biocomputation and Complex Systems Physics Institute (BIFI)-Joint Unit BIFI-IQFR (CSIC), University of Zaragoza, 50018 Zaragoza, Spain; and [g]MedStar–Georgetown Transplant Institute, Georgetown University School of Medicine, Washington, DC 20010

Edited by Gregory A. Petsko, Weill Cornell Medical College, New York, NY, and approved December 5, 2016 (received for review June 29, 2016)

The self-assembly of α-synuclein is closely associated with Parkinson's disease and related syndromes. We show that squalamine, a natural product with known anticancer and antiviral activity, dramatically affects α-synuclein aggregation in vitro and in vivo. We elucidate the mechanism of action of squalamine by investigating its interaction with lipid vesicles, which are known to stimulate nucleation, and find that this compound displaces α-synuclein from the surfaces of such vesicles, thereby blocking the first steps in its aggregation process. We also show that squalamine almost completely suppresses the toxicity of α-synuclein oligomers in human neuroblastoma cells by inhibiting their interactions with lipid membranes. We further examine the effects of squalamine in a *Caenorhabditis elegans* strain overexpressing α-synuclein, observing a dramatic reduction of α-synuclein aggregation and an almost complete elimination of muscle paralysis. These findings suggest that squalamine could be a means of therapeutic intervention in Parkinson's disease and related conditions.

Parkinson's disease | protein aggregation | amyloid formation | toxic oligomers | drug development

The aggregation of α-synuclein (Fig. 1*A*), an intrinsically disordered protein expressed at high levels in the brain, is closely associated with the pathogenesis of a variety of neurodegenerative disorders, collectively known as α-synucleinopathies, including Parkinson's disease (PD), dementia with Lewy bodies (DLB), and multiple-system atrophy (MSA) (1–7). It has been exceptionally challenging, however, to develop effective strategies to suppress the formation of α-synuclein aggregates and their associated toxicity (8, 9), because the mechanism of aggregation of this protein is extremely complex and highly dependent on environmental factors, such as pH, temperature, and contact with surfaces (10). In particular, it is well established that phospholipid binding can accelerate fibril formation (11); moreover, it has recently been shown that such acceleration occurs through the enhancement of the initial primary nucleation step in the aggregation process (12). In the light of this information, we decided to investigate whether compounds capable of altering the binding of α-synuclein to lipid membranes could be effective in inhibiting its aggregation. This study was stimulated by our recent finding that a small molecule, bexarotene, can suppress significantly the primary nucleation reaction that initiates the production of the $A\beta_{42}$ aggregates linked with Alzheimer's disease (AD) and reduces the associated toxicity in a *Caenorhabditis elegans* model of this disease (13).

In the present work, we have focused on one particular compound, squalamine (Fig. 1*B*), an antimicrobial aminosterol originally discovered in 1993 in the dogfish shark, *Squalus acanthias* (14). This small molecule, now prepared synthetically (see *SI Materials and Methods* for details), has been found to have pharmacological activity in endothelial cells by inhibiting growth factor-dependent pathways and thus has emerged as a drug candidate for the treatment of cancer and macular degeneration (15, 16). In the present context, our choice of studying squalamine was prompted by the observation that this molecule is able to enter eukaryotic cells and displace proteins that are bound to the cytoplasmic face of plasma membranes (17–19), suggesting that it may influence the initiation of the aggregation of α-synuclein (12). Indeed squalamine has been referred to as a "cationic lipid" (18) as it carries a net positive charge and shows a high affinity for anionic phospholipids (20) of the type that nucleates the aggregation of α-synuclein, thereby reducing the negative charge of the membrane surface to which it is bound (18, 21) without significantly disrupting the integrity of lipid surfaces (18). In analogy, it has recently been shown that a homologous protein, β-synuclein, can inhibit α-synuclein lipid-induced aggregation via a competitive binding at the surface of lipid vesicles (22).

Significance

Parkinson's disease is characterized by the presence in brain tissues of aberrant aggregates primarily formed by the protein α-synuclein. It has been difficult, however, to identify compounds capable of preventing the formation of such deposits because of the complexity of the aggregation process of α-synuclein. By exploiting recently developed highly quantitative in vitro assays, we identify a compound, squalamine, that blocks α-synuclein aggregation, and characterize its mode of action. Our results show that squalamine, by competing with α-synuclein for binding lipid membranes, specifically inhibits the initiation of the aggregation process of α-synuclein and abolishes the toxicity of α-synuclein oligomers in neuronal cells and in an animal model of Parkinson's disease.

Author contributions: M.P., E.A.A.N., T.P.J.K., M.V., A.B., M.Z., and C.M.D. designed research; M.P., C.G., A.M., G.M., M.B.D.M., P.K.C., J.B.K., P.F., R.C., R.L., P.S., G.T.H., F.A.A., C.C., F.C., T.P.J.K., A.B., and M.Z. performed research; P.K.C., S.W.C., N.C., and E.A.A.N. contributed new reagents/analytic tools; M.P., C.G., A.M., G.M., P.K.C., J.B.K., P.F., S.I.A.C., R.C., R.L., P.S., C.C., F.C., E.A.A.N., T.P.J.K., A.B., M.Z., and C.M.D. analyzed data; and M.P., T.P.J.K., M.V., A.B., M.Z., and C.M.D. wrote the paper.

Conflict of interest statement: M.Z. is the inventor on a patent application that has been filed related to the compound described in this paper. The other authors declare no conflict of interest.

This article is a PNAS Direct Submission.

Freely available online through the PNAS open access option.

[1]Present address: German Center for Neurodegenerative Diseases (DZNE), 53127 Bonn, Germany, and Institute of Physical Biology, Heinrich Heine Universität, Universitätsstr. 1, 40225 Duesseldorf, Germany.

[2]To whom correspondence may be addressed. Email: mv245@cam.ac.uk, bax@nih.gov, maz5@georgetown.edu, or cmd44@cam.ac.uk.

This article contains supporting information online at www.pnas.org/lookup/suppl/doi:10.1073/pnas.1610586114/-/DCSupplemental.

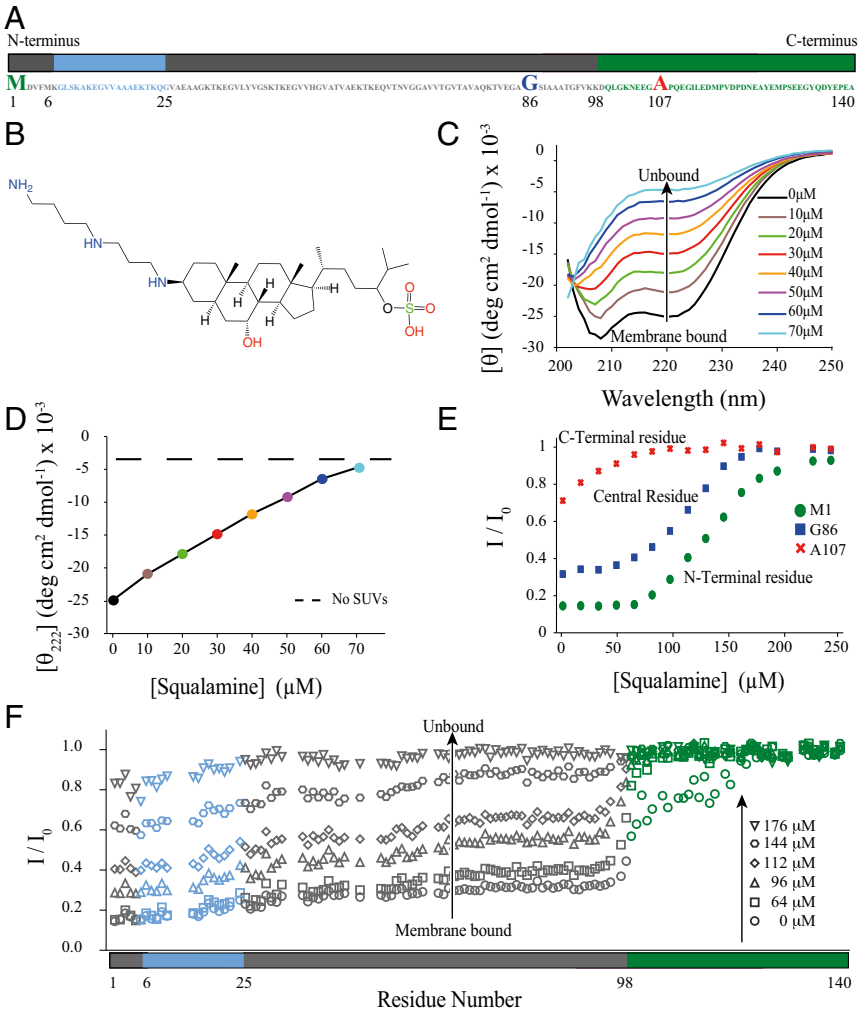

Fig. 1. Squalamine displaces α-synuclein from DOPS:DOPE:DOPC (30:50:20) vesicles. (*A*) Amino acid sequence of α-synuclein and its three distinct regions (44), the N-terminal region (blue), the central region (gray), and the C-terminal fragment (green). (*B*) Structure of squalamine (21). (*C* and *D*) Changes in the CD spectrum (*C*) and the mean residue ellipticity (MRE) (*D*) at 222 nm of 5 μM α-synuclein in the presence of 1.25 mM DOPS:DOPE:DOPC (30:50:20) vesicles in the absence (black) and presence (colors) of increasing concentrations of squalamine: 10 μM (brown), 20 μM (green), 30 μM (red), 40 μM (orange), 50 μM (violet), 60 μM (blue), and 70 μM (light blue) in 20 mM Tris (pH 7.4) and 100 mM NaCl. The dashed horizontal line in *D* indicates the MRE at 222 nm of monomeric α-synuclein in the absence of lipids. Nearly complete displacement of α-synuclein is achieved for a lipid:squalamine ratio of about 18:1. (*E*) Ratios of the α-synuclein NMR peak heights as a function of added squalamine for three residues representative of the three regions of α-synuclein with distinct forms of behavior (11), the N-terminal residue M1 (circles), the central non-Aβ component (NAC) residue G86 (squares), and the C-terminal residue A107 (crosses). (*F*) Ratios of the NMR peak heights of 100 μM of α-synuclein observed in ^{1}H-^{15}N NMR HSQC spectra in the presence of DOPE:DOPS:DOPC (30:50:20) vesicles (1.25 mM) and different concentrations of squalamine (0 μM, circles; 64 μM, squares; 96 μM, triangles; 112 μM, rhomboids; 144 μM, hexagons; and 176 μM, inverted triangles) relative to peak heights in a spectrum of α-synuclein in the absence of lipids and squalamine. Essentially complete displacement of α-synuclein from lipid membranes is observed at a concentration of squalamine of ca. 200 μM, corresponding to a lipid:squalamine ratio of about 6:1. For all the experiments shown in this figure N-terminally acetylated α-synuclein was used (45).

Because of these properties, we investigated the possibility that squalamine could be effective in interfering with the membrane-induced aggregation of α-synuclein. We first investigated the possible mechanism of action of squalamine in this regard by detailed biophysical studies in vitro and extended those results by testing the effects of squalamine on the toxicity of α-synuclein oligomers, using human neuroblastoma cells in culture (23, 24), and then carried out experiments in vivo, using a well-established *C. elegans* animal model of PD (25).

Results

Squalamine Displaces α-Synuclein from Lipid Membranes. To study whether or not squalamine can affect the binding of α-synuclein to lipid bilayers, we first used small unilamellar vesicles (SUVs) with diameters of about 30 nm composed of 30% 1,2-dioleoyl-*sn*-glycero-3-phospho-L-serine (DOPS), 50% 1,2-dioleoyl-*sn*-glycero-3-phosphoethanolamine (DOPE), and 20% 1,2-dioleoyl-*sn*-glycero-3-phosphocholine (DOPC), which represent the most abundant lipids found in the membranes of synaptic vesicles (26). Titrating squalamine into a solution of α-synuclein bound to DOPS:DOPE:DOPC (30:50:20) vesicles was observed to reduce the α-helical content of α-synuclein in an approximately linear manner with squalamine concentration, as measured by circular dichroism (CD) (Fig. 1 *C* and *D*). This observation suggests that squalamine is able to displace α-synuclein from the surface of lipid bilayers.

The physiological concentration of α-synuclein in neuronal synapses is estimated to be about 50 μM (27, 28), a concentration of protein that can be studied by NMR spectroscopy (27, 29–32). We therefore used this technique to probe potential interactions between α-synuclein and squalamine in the absence of lipids and to

characterize the displacement of the protein from lipid membranes by squalamine, as suggested by the CD experiments. This approach is based on the fact that even very weak interactions typically generate measurable shifts in the NMR signals of interacting molecules and often broaden the resonances to an extent that is determined by the rates involved in the binding process.

We first incubated free monomeric α-synuclein in the absence of lipids and in the presence of increasing concentrations of

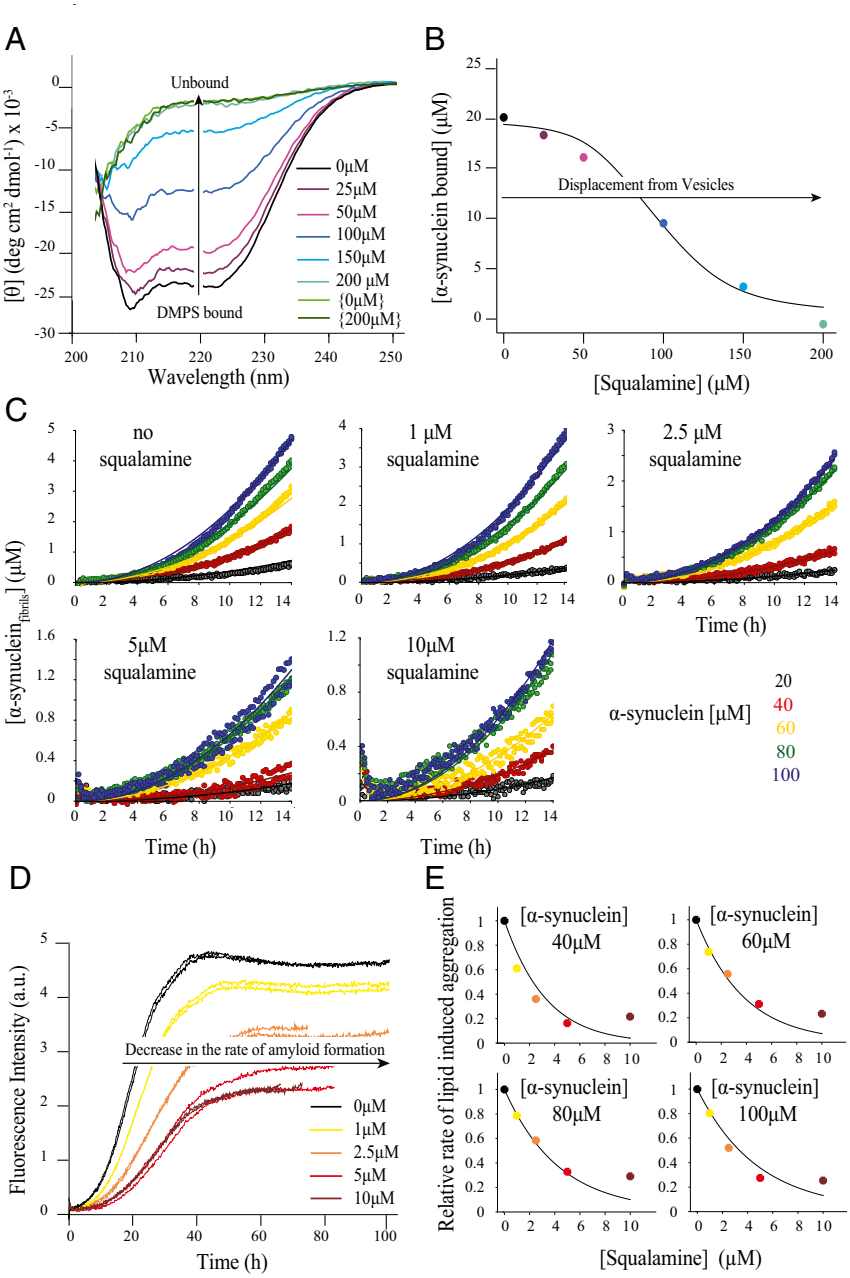

Fig. 2. Squalamine inhibits α-synuclein aggregation via competitive binding with lipid membranes. (*A*) Changes in the CD spectrum of 20 μM α-synuclein in the presence of 1 mM DMPS and in the absence (black) or presence (colors) of increasing concentrations of squalamine: 25 μM (violet), 50 μM (pink), 100 μM (blue), 150 μM (light blue), and 200 μM (aqua). The spectrum of α-synuclein in the absence of both DMPS and squalamine is shown in light green and the CD spectrum of α-synuclein in the absence of DMPS and the presence of 200 μM squalamine is shown in dark green. Essentially complete displacement of the protein from the membrane was observed for a squalamine:lipid ratio of about 1:5. (*B*) Changes in the concentration of α-synuclein bound to DMPS vesicles with increasing concentrations of squalamine. The data are well described by a competitive binding model with $K_{D,\alpha}$ and L_α [0.5 μM and 30 μM, respectively (12)], and the fit yields $K_{D,S}$ = 67 nM and L_S = 7.3, respectively (see *SI Materials and Methods* for details). (*C*) Global fits of the early time points in the kinetic traces of α-synuclein aggregation at increasing concentrations of squalamine. For each dataset, the concentration of DMPS is 100 μM and that of α-synuclein is 20 μM (black), 40 μM (red), 60 μM (yellow), 80 μM (green), and 100 μM (blue). The squalamine concentration used was 0 μM, 1 μM, 2.5 μM, 5 μM, and 10 μM. (*D*) Changes in thioflavin-T (ThT) fluorescence when 100 μM α-synuclein was incubated with 100 μM DMPS vesicles in the presence of increasing concentrations of squalamine: 0 μM (black), 1 μM (yellow), 2.5 μM (orange), 5 μM (red), and 10 μM (brown). All data were acquired under quiescent conditions at 30 °C and duplicate runs are shown. (*E*) Variation in the relative rate of lipid-induced aggregation of α-synuclein with increasing concentrations of squalamine (0 μM, black; 1 μM, yellow; 2.5 μM, orange; 5 μM, red; and 10 μM, brown). The solid line is the corresponding global fit using a competitive binding model (See *SI Materials and Methods* for details) with only one free parameter, n_b (the reaction order of the lipid-induced aggregation with respect to the fraction of the protein bound), which was found to be 5.5.

squalamine and observed small chemical shift changes in the resonances of residues in the C-terminal region of the protein (Fig. S1), consistent with those associated with the weak binding of α-synuclein to other polyamine compounds (33). The interaction involves two regions between residues 85 and 140, where the NMR spectra reveal two distinct types of behavior; the resonances of residues 88–106 show only very small effects, but those of residues 113–139 are affected in a much more pronounced manner. To probe the stoichiometry of the interaction of α-synuclein and squalamine and to estimate the binding constant, we performed a series of dilutions on a sample containing 80 μM α-synuclein and 240 μM squalamine, monitoring the intensities of the α-synuclein resonances (Fig. S1). This experiment shows that when the squalamine concentration becomes lower than about 100 μM, the spectral changes characteristic of the interaction are no longer visible.

Then, we investigated further the displacement of α-synuclein from the membrane by squalamine. It has been previously demonstrated that addition of DOPE:DOPS:DOPC (50:30:20) vesicles to a sample of α-synuclein results in attenuation of the main-chain amide signals of its about 100 N-terminal residues in the ^{1}H-^{15}N heteronuclear single quantum correlation (HSQC) NMR spectrum (27). This attenuation is attributable to the binding of these residues to the large, slowly tumbling vesicles, whereas the secondary structure becomes α-helical, as indicated by CD measurements and by indirect transferred nuclear Overhauser effects (NOEs) in the spectra (27). By contrast, the resonances of the 40 C-terminal residues retain almost their full intensity and experience only very minor changes in chemical shifts (Fig. 1*F*). In the present work we prepared an NMR sample containing a sufficient quantity of lipid vesicles to cause a large attenuation of the signals of α-synuclein and then titrated increasing amounts of squalamine into the sample (Fig. 1 *E* and *F*). We observed that the addition of about 200 μM of squalamine resulted in an almost complete recovery of the intensity of the α-synuclein signals (Fig. 1*F*) and found that signals from residues 101–120, which are affected to a much smaller extent than residues 1–100 by the presence of lipids, were restored to their free intensities at a much lower concentration of squalamine.

Interestingly, even though the squalamine:α-synuclein ratios and the absolute squalamine concentrations in the presence of DOPE:DOPS:DOPC vesicles (Fig. 1 *C* and *D*) were comparable to those in the lipid-free experiments (Fig. S1), there was no evidence in the former experiments for the interaction of squalamine with the C-terminal residues. In addition, when the squalamine concentration was increased to 80 μM in the absence

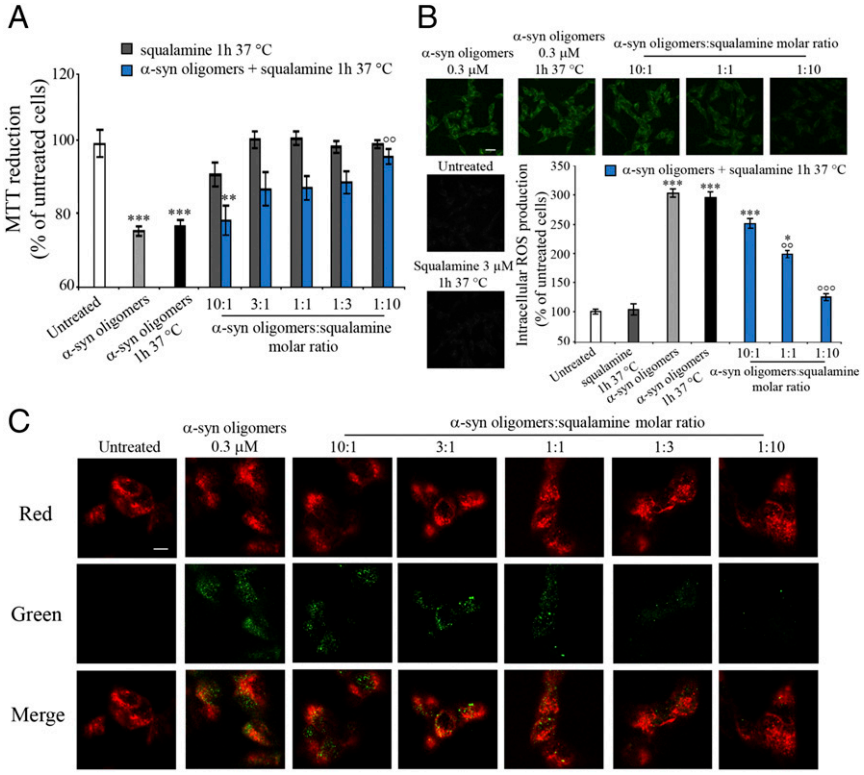

Fig. 3. Squalamine suppresses the toxicity of α-synuclein oligomers in human neuroblastoma cells by inhibiting their binding to the cell membranes. (*A*) Effects of squalamine on α-synuclein oligomer-induced MTT reduction in SH-SY5Y cells. α-Synuclein oligomers (23, 24) were resuspended in the cell culture medium at a concentration of 0.3 μM, incubated with or without increasing concentrations (0.03 μM, 0.1 μM, 0.3 μM, 1.0 μM, and 3.0 μM) of squalamine for 1 h at 37 °C under shaking conditions, and then added to the cell culture medium of SH-SY5Y cells for 24 h. The cells were also treated with squalamine preincubated in the absence of oligomers for 1 h at 37 °C under shaking conditions. $^{**}P \leq 0.01$ and $^{***}P \leq 0.001$, respectively, relative to untreated cells and $^{\circ\circ}P \leq 0.01$ relative to cells treated with α-synuclein oligomers. (*B*) Representative confocal scanning microscope images of SH-SY5Y cells showing the effect of squalamine on α-synuclein oligomer-induced ROS production. α-Synuclein oligomers were resuspended in the cell culture medium at a concentration of 0.3 μM, incubated with or without increasing concentrations (0.03 μM, 0.3 μM, and 3.0 μM) of squalamine for 1 h at 37 °C under shaking conditions, and then added to the cell culture medium of SH-SY5Y cells for 15 min. The cells were also treated with 3 μM squalamine preincubated without oligomers for 1 h at 37 °C while shaking. The green fluorescence arises from the 2′,7′-dichlorodihydrofluorescein diacetate (CM-H_2DCFDA) probe that has reacted with ROS. (Scale bar, 30 μm.) $^{*}P \leq 0.05$, $^{**}P \leq 0.01$, and $^{***}P \leq 0.001$, respectively, relative to untreated cells. $^{\circ\circ}P \leq 0.01$ and $^{\circ\circ\circ}P \leq 0.001$, respectively, relative to untreated cells and the symbol °° indicates $P \leq 0.01$ relative to cells treated with α-synuclein oligomers. (*C*) Representative confocal scanning microscopy images of the apical sections of SH-SY5Y cells treated for 15 min with α-synuclein oligomers (0.3 μM) and increasing concentrations (0.03 μM, 0.1 μM, 0.3 μM, 1.0 μM, and 3.0 μM) of squalamine. Red and green fluorescence indicates the cell membranes and the α-synuclein oligomers, respectively. (Scale bar, 10 μm.)

of α-synuclein, the sample became highly opaque, suggesting that the lipid vesicles in the sample undergo fusion within seconds, an effect likely to be due to the change in the electrostatic properties of the lipid vesicles upon squalamine binding. However, in the presence of α-synuclein the samples were stable and no precipitation occurred within the time scales of either the CD or the NMR experiments.

Taken together, these observations demonstrate that, in a system containing α-synuclein and negatively charged lipid membranes, squalamine partitions to the membrane surface, thereby inducing the displacement of the protein from the membrane rather than remaining free in solution and interacting directly with α-synuclein.

Squalamine Inhibits Lipid-Induced Aggregation of α-Synuclein by Competing for Binding Sites at the Surface of the DMPS Vesicles. In the light of these results, we explored the effects of squalamine on the binding and aggregation of α-synuclein in the presence of 1,2-dimyristoyl-sn-glycero-3-phospho-L-serine (DMPS)-containing vesicles, which have been shown to be particularly effective in enhancing the rate of aggregation and amyloid formation by α-synuclein (12). We first incubated the protein under conditions where effectively all of the α-synuclein molecules present in the sample were bound to the vesicles and in the presence of increasing concentrations of squalamine. As observed in the experiments with the DOPS:DOPE:DOPC (30:50:20) vesicles (Fig. 1 *C*–*F*), the presence of squalamine progressively decreased the α-helical content of α-synuclein (Fig. 2*A*), again indicating that squalamine displaces the protein from the vesicles. We thus used the same competitive binding model (Fig. 2*B*) as the one describing the displacement of α-synuclein from the vesicle by β-synuclein (22), where both α-synuclein and squalamine compete for binding sites at the surface of the DMPS vesicles, in order to analyze the CD data. This model, together with previously determined binding constants for the α-synuclein/DMPS system (12), described the data very closely and yielded values for both the binding constant and the stoichiometry of the binding of squalamine to DMPS vesicles, $K_{D,S} = 67$ nM and $L_S = 7.3$, respectively. These results suggest that the positively charged squalamine binds strongly to the anionic head groups of the lipid bilayers, progressively coating the surfaces of the lipid membrane, thereby decreasing the electrostatic forces and competing for the sites on the lipid vesicles that are required for the binding of α-synuclein.

We further monitored the effects of increasing concentrations of squalamine on the size and the fluidity of the DMPS vesicles, using dynamic light scattering and differential scanning calorimetry (Fig. S2), respectively. The presence of squalamine caused an increase in the diameter of the DMPS vesicles from about 20 nm to values in excess of 100 nm at squalamine:lipid ratios greater than 0.1 (Fig. S2). In addition, differential scanning calorimetry

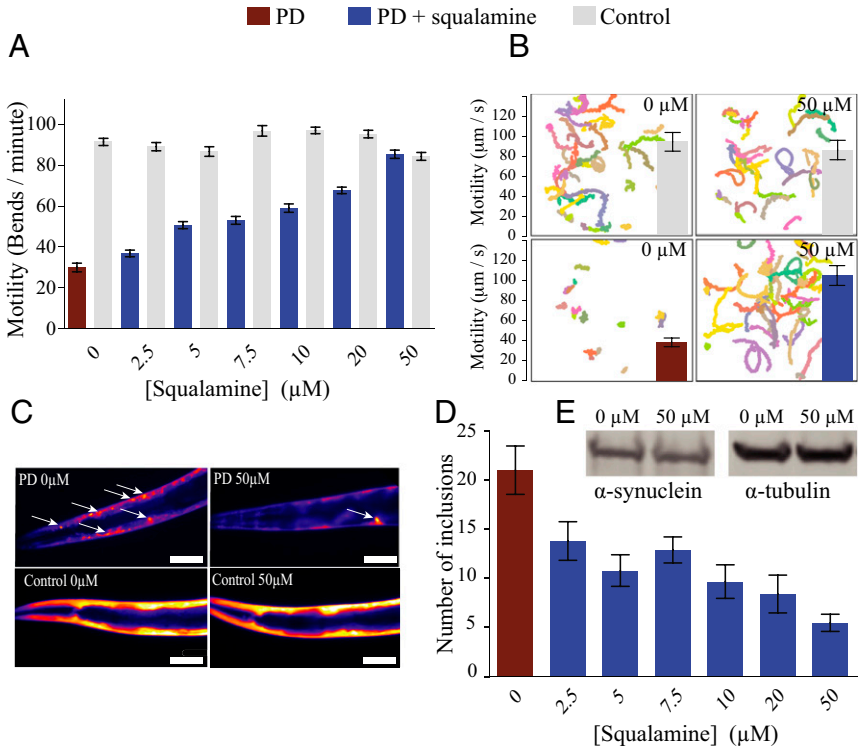

Fig. 4. Squalamine inhibits the formation of α-synuclein inclusions and the consequent muscle paralysis associated with the overexpression of this protein in a *C. elegans* model of PD. (*A*) Recovery of the normal phenotype at day 4 of adulthood for PD worms (red bars) and for worms expressing α-synuclein (blue bars) compared with control worms (gray bars) as the concentration of squalamine was raised to 50 μM. The data were obtained using an automated body bend assay; the plot shows one representative dataset of three independent experiments that gave very similar results. (*B*) Swimming tracks representative of the movement of PD and control worms over a time period of 1 min, without and with squalamine. Tracks corresponding to the movement of different animals are represented in different colors. The motility (speed of movement and body bends) of the PD worms can be seen to be greatly enhanced after exposure to 50 μM squalamine. Red bars, PD worms; blue bars, treated PD worms; gray bars, control worms. The error bars represent the SEM. (*C*) Representative images, showing a substantial decrease in the number of inclusions in PD worms in the presence of 50 μM squalamine, whereas the YFP expression pattern in control worms is not affected. All measurements were carried out at day 12 of adulthood. (Scale bars, 70 μm.) Inclusions are indicated with white arrows. (*D*) Reduction in the number of α-synuclein inclusions in PD worms, in the presence of squalamine. Fifty animals were analyzed in total. Red bar, PD worms; blue bars, treated PD worms. (*E*) Western blot analysis of protein extracts from day 12 PD worms showing similar expression levels of α-synuclein and α-tubulin (loading control) in the absence and presence of 50 μM squalamine.

(DSC) traces of the DMPS vesicles in the absence and presence of 50 μM squalamine show that the molecule induced a decrease in the melting temperature by 10 °C (Fig. S2), an effect similar to that observed upon binding of α-synuclein to DMPS vesicles (12), suggesting that squalamine interacts with the membrane surface. Overall, however, these results indicate that at squalamine:DMPS ratios below 1:10 the integrity of the vesicles is not compromised.

We then studied the aggregation of α-synuclein in the presence of DMPS vesicles and increasing concentrations of squalamine and observed that the overall rate of amyloid formation under such conditions decreases dramatically in a dose-dependent manner (Fig. 2 *C–E*). It is interesting to note that the observed change in the rate of lipid-induced aggregation of α-synuclein is not likely to be due to a change in the vesicle morphology; as discussed above, at the squalamine:lipid ratios used here the diameter of the vesicles ranges from 20 nm to 100 nm (Fig. S2), and this size variation has been shown not to affect significantly the kinetics of amyloid formation by α-synuclein in the presence of DMPS vesicles (12).

To quantify further the effects of squalamine on α-synuclein aggregation, we analyzed the early stages of the kinetic traces (Fig. 2*C*) (12) (see *SI Materials and Methods* for details) and determined the rate of α-synuclein aggregation at each concentration of squalamine (Fig. 2*E*). The change in the relative rate of lipid-induced aggregation of α-synuclein with increasing concentration of squalamine is well described by a competitive binding model, with the binding constants determined here for squalamine ($K_{D,S}$ and L_S) and previously for α-synuclein ($K_{D,\alpha}$ and L_α) (12). Taken together, these results are consistent with the conclusion that squalamine inhibits the lipid-induced aggregation of α-synuclein via competitive binding at the surfaces of the vesicles, as observed for β-synuclein (22). In addition, we probed the interaction of squalamine with α-synuclein fibrils by incubating squalamine in the presence of the fibrils. We then centrifuged the sample and separated the supernatant from the pellet. Then we assessed the quantity of squalamine in the supernatant before and after incubation with fibrils using, mass spectrometry (Fig. S3). We found that, after incubation, the signal corresponding to squalamine in the supernatant was reduced (−85%), suggesting a degree of binding to α-synuclein fibrils. This interaction may also play a role in the observed inhibition of squalamine on the lipid-induced aggregation of α-synuclein. As a control we performed the same experiment, using $A\beta_{42}$ fibrils (Fig. S3). In this case, we observed a lower binding signal (−66%), indicating stronger binding to α-synuclein fibrils.

Squalamine Suppresses the Toxicity of α-Synuclein Oligomers in Human Neuroblastoma Cell Lines by Inhibiting Their Binding to Cellular Membranes. We have recently developed a protocol to isolate oligomers of α-synuclein shown to be toxic to human cells (23, 24). We exposed cultured human SH-SY5Y neuroblastoma culture cells to such oligomers at a concentration of 0.3 μM (monomer equivalent of α-synuclein). Under these conditions, the oligomers were indeed toxic to the cells, as demonstrated by the decreased ability of the cells to chemically reduce 3-(4,5-dimethylthiazol-2-yl)-2,5-diphenyltetrazolium bromide (MTT) (Fig. 3*A*). The cells were also treated with α-synuclein oligomers (0.3 μM) in the presence of increasing concentrations of squalamine (up to 3.0 μM) (Fig. 3*A*). The results show that squalamine decreases markedly the mitochondrial damage induced by the α-synuclein

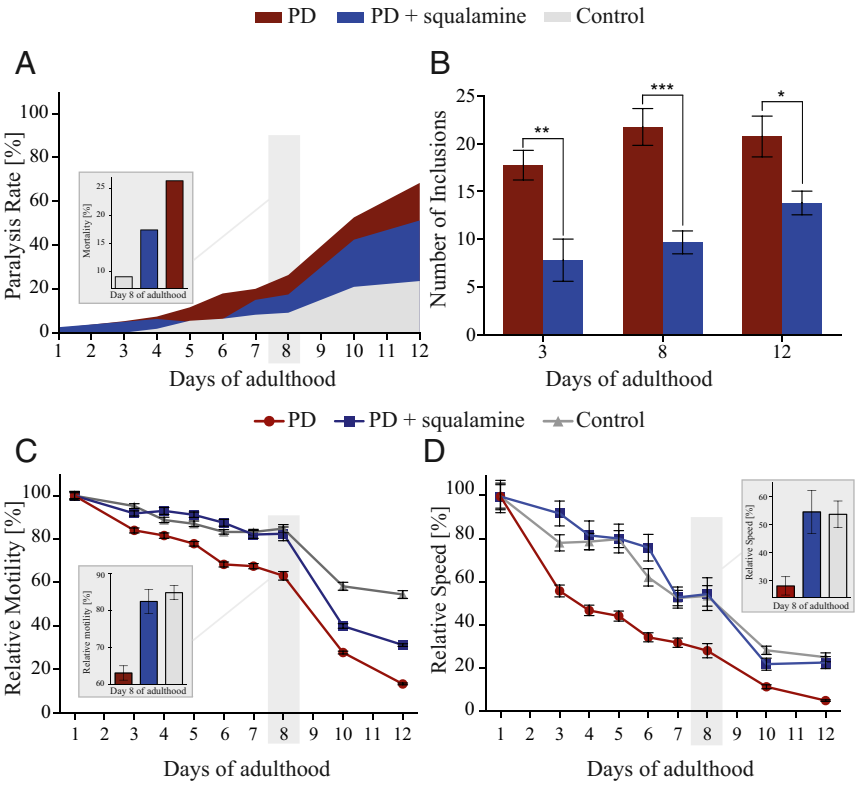

Fig. 5. Squalamine greatly improves the fitness of PD worms (25) and reduces α-synuclein aggregation over time. (*A*) The administration of 10 μM squalamine decreased substantially the paralysis rate of PD worms. Red, PD worms; blue, treated PD worms; gray, control worms. (*B*) The aggregation of α-synuclein in PD animals treated with 10 μM squalamine is greatly decreased compared with that in untreated worms; the plots show one representative of three experiments. Error bars represent the SEM. Red bars, PD worms; blue bars, treated PD worms. (*C* and *D*) Exposure to 10 μM squalamine greatly improves the thrashing (*C*) and speed (*D*) of the PD worms over 12 d. *Insets* show details of relative motility, thrashing, and speed, respectively, for day 8. Red lines, PD worms; blue lines, treated PD worms; gray lines, control worms.

oligomers, as indicated by MTT reduction data, with the protective effect increasing with squalamine concentration (Fig. 3*A*). Similar results were obtained from analyzing intracellular reactive oxygen species (ROS) production within SH-SY5Y cells; the α-synuclein oligomers (0.3 μM) induced a sharp increase in ROS levels in this cell model, indicating increased ROS-induced cellular damage (Fig. 3*B*). Upon treatment of the cells with α-synuclein oligomers (0.3 μM monomer equivalent) and increasing concentrations (0.03 μM, 0.3 μM, and 3 μM) of squalamine, the degree of ROS-derived fluorescence was observed to decrease steadily with increasing squalamine concentration (Fig. 3*B*), and at the highest ratio of squalamine:α-synuclein concentrations it was found to suppress almost completely the increase of intracellular ROS levels caused by the oligomers.

We then investigated the mechanism by which squalamine inhibits α-synuclein oligomer toxicity by analyzing the interactions between the oligomers (0.3 μM) and human SH-SY5Y neuroblastoma cells at increasing concentrations (up to 3.0 μM) of squalamine, using confocal microscopy and anti–α-synuclein antibodies. The images were scanned at apical planes to detect oligomers (green channel) interacting with the cellular surface (red channel) (Fig. 3*C*). Large numbers of α-synuclein oligomers bound to the plasma membrane were observed in cells exposed to oligomers, but their number was markedly decreased as the squalamine concentration was increased (Fig. 3*C*). As we have shown previously, the toxicity caused by protein oligomers can be correlated with membrane binding (34) and this finding provides an explanation for the inhibition of the cellular damage induced by α-synuclein oligomers by squalamine and is consistent with a competitive binding model.

Squalamine Reduces α-Synuclein Aggregation and Related Paralysis in a Worm Model of PD. We extended our in vitro observations that squalamine can suppress the aggregation and toxicity of α-synuclein to a living system. We used a well-studied model of PD in the nematode worm *C. elegans*, which is based on the overexpression of α-synuclein tagged with yellow fluorescent protein (YFP) in the muscle cells of the nematode worms (25). This model organism, in which the presence of α-synuclein causes characteristic phenotypic changes (25), has been successfully used to probe the nature of a range of neurodegenerative conditions and has been used in high-throughput screens to identify novel genes that modify the course of disease (35, 36).

Motility in *C. elegans* declines during aging and it can be measured in liquid media by counting the number of body bends per unit of time (37). This phenotypic readout has been used extensively for identification of genes and pathways connected to age-related protein homeostasis, as well as for the definition of modifiers of protein aggregation (25, 35, 36); both of these processes are closely associated with the onset and development of neurodegenerative diseases (5, 7, 38). We first tested different approaches to optimize the effects of squalamine in vivo and found that the best treatment regime was to administer the compound at the larval stage L4, when the worms were fully developed, and to maintain the worms on plates seeded with squalamine for their whole lifespan. By carrying out standard

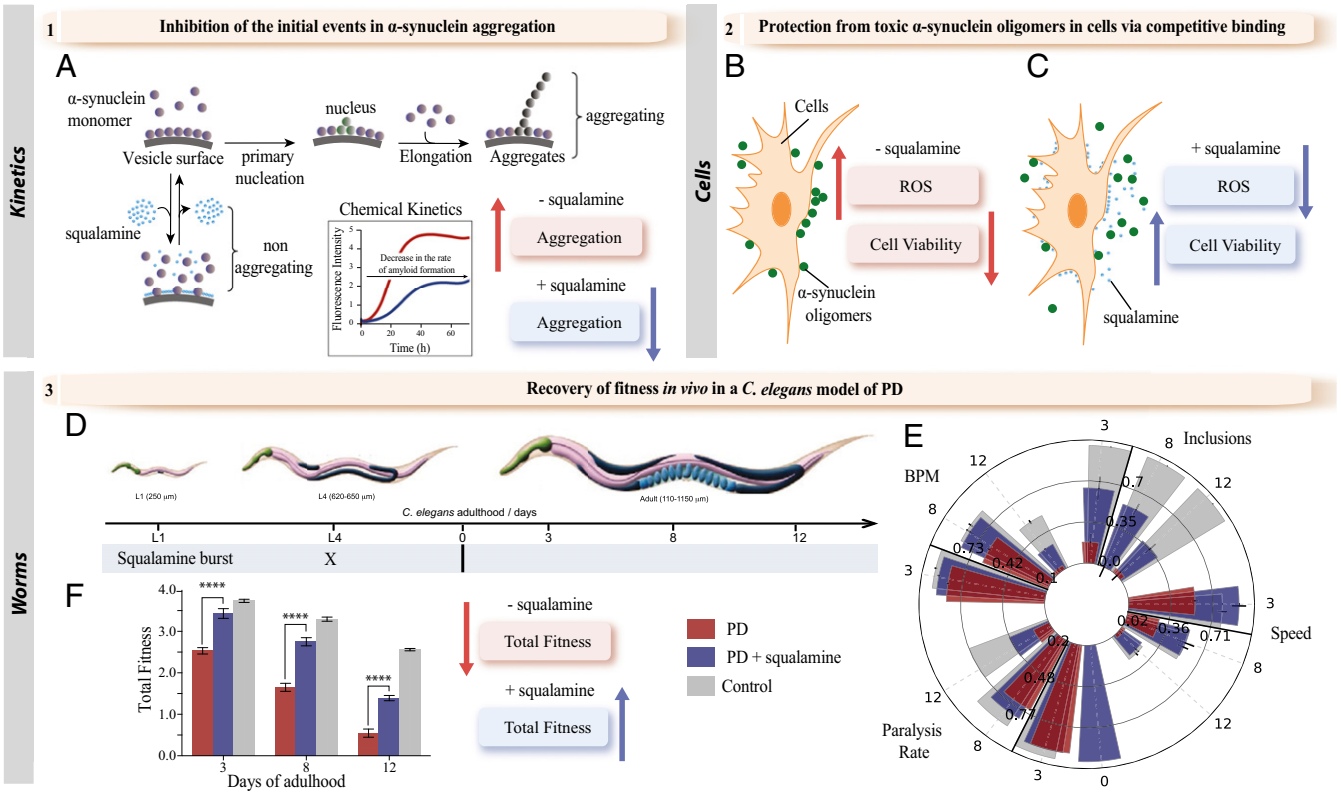

Fig. 6. Schematic illustration of the drug discovery strategy used in this work. (*A*) We used a wide range of biophysical techniques, including chemical kinetics, to study quantitatively the effects of squalamine on α-synuclein aggregation in vitro and we observed that squalamine affects the binding of α-synuclein to lipid membranes and inhibits the initial events in its aggregation. (*B* and *C*) By using the protocols that we recently developed to isolate oligomers of α-synuclein toxic to human cells (23, 24), we have shown that squalamine inhibits dramatically the mitochondrial dysfunction and cellular ROS production induced by the oligomers of α-synuclein (23, 24). (*D*–*F*) We further validated our results in vivo by using a well-established *C. elegans* model of PD (25), and we found that administration of a single dose of squalamine at the larval stage L4 (*D*) abolishes α-synuclein aggregation and its associated toxicity in vivo over several days (*E*) and increases the total fitness of the PD worms (*F*).

body bend assays (37), we observed a very significantly improved motility of the PD worms treated with squalamine (Fig. S4). By contrast, the motility of a *C. elegans* strain expressing only YFP, used here as a control, was not detectably affected by squalamine (Fig. S4).

As standard body bend assays monitored by manual means can be prone to errors and are not always reproducible, many digital tracking platforms have recently been proposed to characterize worm behavior in a more quantitative and rigorous way (39). To improve the reproducibility of the results, we have developed a high-throughput microscopic screening procedure that allows robust *C. elegans* phenotypic screening with improved statistics, coupled with automated analysis of the motility of the animals (see *SI Materials and Methods* for details).

Movies of swimming worms were recorded using a high-performance imaging lens and a machine vision camera at a high number of frames per second (fps) for 30 s or 1 min, and the platform enabled us to image simultaneously up to 200 swimming animals over the whole surface of a 6-cm agar plate (see *SI Materials and Methods* for details). Using this method, we confirmed with statistical confidence the observed improved motility (Fig. S5) of the PD worms upon squalamine administration (Figs. 4*A*, 5, and 6 and Movies S1–S4). Automated analysis of the velocities of the movements of the worms further confirmed a significant difference between treated and untreated PD worms, and indeed those animals exposed to 50 μM squalamine showed motility levels that were essentially the same as those of the control worms (Fig. 4*B*).

We then explored the effects of squalamine on the aggregation of α-synuclein in PD worms by fluorescence microscopy. Following the addition of squalamine to the medium in which the animals were maintained, we observed a substantial decrease in α-synuclein inclusion formation in aged PD worms (day 12 of adulthood) (Fig. 4 *C* and *D*), despite the fact that the levels of α-synuclein expression in the PD worms in the absence and in the presence of squalamine were found to be closely similar (Fig. 4*E*). We also demonstrated that no effects could be detected on the intensity or the distribution pattern of YFP expressed within the body-wall muscle of the control worms (Fig. 4*C*).

Furthermore the protective effect of squalamine was apparent throughout the study, as shown by recovery of motility (thrashing and speed), decrease in paralysis rate, and the decrease in the number of inclusions (Fig. 5). Finally, to assess whether or not the observed effects of squalamine in suppressing inclusion formation and toxicity were specific to the α-synuclein worms, we tested squalamine in a worm model of $A\beta_{42}$-mediated dysfunction (40). In this system, where the presence of lipids is not required for the initiation of $A\beta_{42}$ aggregation (41, 42), we observed that squalamine, at concentrations that completely restored the pathological phenotype in the $Abeta^{42}$ worms, showed no significant protective effects (Fig. S5), thereby indicating the specificity of squalamine against α-synuclein aggregation.

Discussion

We have shown by using a variety of biophysical techniques that squalamine can inhibit in vitro the aggregation of α-synuclein induced by lipid membranes. Furthermore we have shown by using a cellular model and an animal model of PD that squalamine dramatically reduces in vivo the toxicity associated with α-synuclein aggregation (Fig. 6).

To study the binding of α-synuclein to lipids, we first used SUVs composed of DOPS, DOPE, and DOPC, which are the most abundant lipids found in the membranes of synaptic vesicles (26). Titrating squalamine into a solution of α-synuclein bound to SUVs caused the α-helical content of α-synuclein to decrease in an approximately linear manner with squalamine concentration, as measured by CD and NMR, thus suggesting that squalamine displaces α-synuclein from lipid membranes, as observed for a range of other protein/lipid systems (17). We further explored the effects of squalamine on the binding and aggregation of α-synuclein in the presence of DMPS-containing vesicles, which have been shown to be particularly effective in enhancing the rate of aggregation and amyloid formation of α-synuclein (12). The presence of squalamine progressively decreased the α-helical content of α-synuclein, again indicating that this compound displaces the protein from the vesicles, as recently observed for β-synuclein (22). To analyze these data, we thus used the same competitive binding model as the one describing the inhibitory effect of β-synculein on α-synuclein lipid-induced aggregation (22), where both α-synuclein and squalamine compete for binding sites at the surface of the DMPS vesicles, which validated the model in a quantitative manner.

In addition, we have shown that squalamine does not interact directly with monomeric α-synuclein in free solution, except at very high concentrations and in the absence of lipids, and that it affects the size and the thermotropic properties of lipid vesicles only at high squalamine:DMPS ratios (>0.1). Moreover, we have observed that the overall rate of lipid-induced α-synuclein aggregation in vitro decreases dramatically and in a dose-dependent manner upon incubation with squalamine.

We then extended this study by using SH-SY5Y cells treated with oligomers of α-synuclein previously shown to be toxic to cells in culture (23, 24) and found that squalamine inhibits completely the mitochondrial dysfunction and the cellular ROS production induced by the oligomers. The degree of binding of toxic α-synuclein oligomers to neuronal cells also decreased with increasing squalamine concentration, and based on our results, we proposed a competitive binding model, where toxic oligomers of α-synuclein and squalamine compete for binding sites at the surface of neuronal cells. These results suggest that squalamine drastically decreases not only the neurotoxicity caused by the intracellular accumulation of α-synuclein aggregates but also the cellular damage induced by aggregates interacting with the membrane of neuronal cells. We then provided further evidence for a protective effect of squalamine observed in vitro and in cells by using a well-studied *C. elegans* model of PD (25). When worms were exposed to squalamine from an early stage in their development, we observed an almost complete recovery of the motility dysfunction induced by α-synuclein together with a substantial decrease in inclusion formation in treated PD worms.

Taken together, these results suggest that squalamine inhibits the initial step in the lipid-induced aggregation of α-synuclein through competitive binding at the surface of the lipid vesicles and also drastically reduces the toxicity of oligomeric forms of α-synuclein in vivo. We note that it is also possible that other secondary mechanisms of action, such as direct interactions with fibrils, may be present and could work in synergy with the principal mechanism of action of squalamine that we have described.

Conclusions

We have shown that in vitro and in cell cultures squalamine suppresses the initial events in the aggregation of α-synuclein by displacing the protein from lipid membranes, where such events preferentially take place, and also acts to reduce the interactions of oligomeric aggregates with the membrane surfaces (Fig. 6). These results indicate the mechanisms by which squalamine significantly inhibits the aggregation of α-synuclein in vivo and also reduces dramatically its associated toxicity. We suggest, therefore, that squalamine, and by extension other molecules that can compete effectively with α-synuclein for lipid membrane binding, could have the potential to act as therapeutic agents for PD and other conditions associated with the pathogenic aggregation of α-synuclein.

Materials and Methods

Extended experimental procedures are described in *SI Materials and Methods*. Wild-type α-synuclein was expressed in *Escherichia coli* and purified as previously described (10). DOPE/DOPS/DOPC vesicles were prepared as previously described (27). DMPS vesicles were prepared as previously reported (12) and

aggregation kinetics and related data analysis were carried out as previously described (12). α-Synuclein oligomers were also prepared as described previously (23, 24) and cell cytotoxicity assays were carried out as indicated (43). In vivo experiments were carried out by using a well-studied *C. elegans* model of PD (25).

ACKNOWLEDGMENTS. The authors thank Alfonso de Simone, Sam Casford, Mandy Koopman, and Maarten C. Hardenberg for valuable advice and discussions. This work was supported by the Intramural Research Program of the National Institute of Diabetes and Digestive and Kidney Diseases (NIDDK), US National Institutes of Health (A.M. and A.B.); by the Boehringer Ingelheim Fonds (P.F.); by a European Research Council starting grant (to M.B.D.M. and E.A.A.N.); and by The Cambridge Centre for Misfolding Diseases. N.C. thanks the Spanish Ministry of Economy and Competitiveness (RYC-2012-12068). S.W.C. thanks the Agency for Science, Technology, and Research, Singapore for support.

1. Breydo L, Wu JW, Uversky VN (2012) A-synuclein misfolding and Parkinson's disease. *Biochim Biophys Acta* 1822(2):261–285.
2. Dettmer U, Selkoe D, Bartels T (2016) New insights into cellular α-synuclein homeostasis in health and disease. *Curr Opin Neurobiol* 36:15–22.
3. Spillantini MG, Crowther RA, Jakes R, Hasegawa M, Goedert M (1998) alpha-Synuclein in filamentous inclusions of Lewy bodies from Parkinson's disease and dementia with lewy bodies. *Proc Natl Acad Sci USA* 95(11):6469–6473.
4. Dawson TM, Dawson VL (2003) Molecular pathways of neurodegeneration in Parkinson's disease. *Science* 302(5646):819–822.
5. Knowles TPJ, Vendruscolo M, Dobson CM (2014) The amyloid state and its association with protein misfolding diseases. *Nat Rev Mol Cell Biol* 15(6):384–396.
6. Gómez-Tortosa E, Ingraham AO, Irizarry MC, Hyman BT (1998) Dementia with Lewy bodies. *J Am Geriatr Soc* 46(11):1449–1458.
7. Chiti F, Dobson CM (2006) Protein misfolding, functional amyloid, and human disease. *Annu Rev Biochem* 75(1):333–366.
8. Tóth G, et al. (2014) Targeting the intrinsically disordered structural ensemble of α-synuclein by small molecules as a potential therapeutic strategy for Parkinson's disease. *PLoS One* 9(2):e87133.
9. Lee VMY, Trojanowski JQ (2006) Mechanisms of Parkinson's disease linked to pathological alpha-synuclein: New targets for drug discovery. *Neuron* 52(1):33–38.
10. Buell AK, et al. (2014) Solution conditions determine the relative importance of nucleation and growth processes in α-synuclein aggregation. *Proc Natl Acad Sci USA* 111(21):7671–7676.
11. Fink AL (2006) The aggregation and fibrillation of alpha-synuclein. *Acc Chem Res* 39(9):628–634.
12. Galvagnion C, et al. (2015) Lipid vesicles trigger α-synuclein aggregation by stimulating primary nucleation. *Nat Chem Biol* 11(3):229–234.
13. Habchi J, et al. (2016) An anticancer drug suppresses the primary nucleation reaction that initiates the production of the toxic Aβ42 aggregates linked with Alzheimer's disease. *Sci Adv* 2(2):e1501244.
14. Moore KS, et al. (1993) Squalamine: An aminosterol antibiotic from the shark. *Proc Natl Acad Sci USA* 90(4):1354–1358.
15. Li D, Williams JI, Pietras RJ (2002) Squalamine and cisplatin block angiogenesis and growth of human ovarian cancer cells with or without HER-2 gene overexpression. *Oncogene* 21(18):2805–2814.
16. Genaidy M, et al. (2002) Effect of squalamine on iris neovascularization in monkeys. *Retina* 22(6):772–778.
17. Yeung T, et al. (2008) Membrane phosphatidylserine regulates surface charge and protein localization. *Science* 319(5860):210–213.
18. Sumioka A, Yan D, Tomita S (2010) TARP phosphorylation regulates synaptic AMPA receptors through lipid bilayers. *Neuron* 66(5):755–767.
19. Alexander RT, et al. (2011) Membrane surface charge dictates the structure and function of the epithelial Na+/H+ exchanger. *EMBO J* 30(4):679–691.
20. Selinsky BS, Smith R, Frangiosi A, Vonbaur B, Pedersen L (2000) Squalamine is not a proton ionophore. *Biochim Biophys Acta* 1464(1):135–141.
21. Zasloff M, et al. (2011) Squalamine as a broad-spectrum systemic antiviral agent with therapeutic potential. *Proc Natl Acad Sci USA* 108(38):15978–15983.
22. Brown JWP, et al. (2016) β-Synuclein suppresses both the initiation and amplification steps of α-synuclein aggregation via competitive binding to surfaces. *Sci Rep* 6:36010.
23. Cremades N, et al. (2012) Direct observation of the interconversion of normal and toxic forms of α-synuclein. *Cell* 149(5):1048–1059.
24. Chen SW, et al. (2015) Structural characterization of toxic oligomers that are kinetically trapped during α-synuclein fibril formation. *Proc Natl Acad Sci USA* 112(16):E1994–E2003.
25. van Ham TJ, et al. (2008) C. elegans model identifies genetic modifiers of α-synuclein inclusion formation during aging. *PLoS Genet* 4(3):e1000027.
26. Takamori S, et al. (2006) Molecular anatomy of a trafficking organelle. *Cell* 127(4):831–846.
27. Bodner CR, Dobson CM, Bax A (2009) Multiple tight phospholipid-binding modes of alpha-synuclein revealed by solution NMR spectroscopy. *J Mol Biol* 390(4):775–790.
28. Wilhelm BG, et al. (2014) Composition of isolated synaptic boutons reveals the amounts of vesicle trafficking proteins. *Science* 344(6187):1023–1028.
29. Bussell R, Jr, Eliezer D (2004) Effects of Parkinson's disease-linked mutations on the structure of lipid-associated alpha-synuclein. *Biochemistry* 43(16):4810–4818.
30. Eliezer D, Kutluay E, Bussell R, Jr, Browne G (2001) Conformational properties of α-synuclein in its free and lipid-associated states. *J Mol Biol* 307(4):1061–1073.
31. Kosten J, et al. (2014) Efficient modification of alpha-synuclein serine 129 by protein kinase CK1 requires phosphorylation of tyrosine 125 as a priming event. *ACS Chem Neurosci* 5(12):1203–1208.
32. Serber Z, et al. (2006) Investigating macromolecules inside cultured and injected cells by in-cell NMR spectroscopy. *Nat Protoc* 1(6):2701–2709.
33. Fernández CO, et al. (2004) NMR of alpha-synuclein-polyamine complexes elucidates the mechanism and kinetics of induced aggregation. *EMBO J* 23(10):2039–2046.
34. Evangelisti E, et al. (2016) Binding affinity of amyloid oligomers to cellular membranes is a generic indicator of cellular dysfunction in protein misfolding diseases. *Sci Rep* 6:32721.
35. van Ham TJ, et al. (2010) Identification of MOAG-4/SERF as a regulator of age-related proteotoxicity. *Cell* 142(4):601–612.
36. van der Goot AT, et al. (2012) Delaying aging and the aging-associated decline in protein homeostasis by inhibition of tryptophan degradation. *Proc Natl Acad Sci USA* 109(37):14912–14917.
37. Gidalevitz T, Krupinski T, Garcia S, Morimoto RI (2009) Destabilizing protein polymorphisms in the genetic background direct phenotypic expression of mutant SOD1 toxicity. *PLoS Genet* 5(3):e1000399.
38. Soto C (2003) Unfolding the role of protein misfolding in neurodegenerative diseases. *Nat Rev Neurosci* 4(1):49–60.
39. Husson SJ, Costa WS, Schmitt C, Gottschalk A (2013) Keeping track of worm trackers. *WormBook* 1–17.
40. Link CD (1995) Expression of human beta-amyloid peptide in transgenic Caenorhabditis elegans. *Proc Natl Acad Sci USA* 92(20):9368–9372.
41. Cohen SIA, et al. (2013) Proliferation of amyloid-β42 aggregates occurs through a secondary nucleation mechanism. *Proc Natl Acad Sci USA* 110(24):9758–9763.
42. Scherzinger E, et al. (1999) Self-assembly of polyglutamine-containing huntingtin fragments into amyloid-like fibrils: Implications for Huntington's disease pathology. *Proc Natl Acad Sci USA* 96(8):4604–4609.
43. Cascella R, et al. (2013) Extracellular chaperones prevent Aβ42-induced toxicity in rat brains. *Biochim Biophys Acta* 1832(8):1217–1226.
44. Fusco G, et al. (2014) Direct observation of the three regions in α-synuclein that determine its membrane-bound behaviour. *Nat Commun* 5:3827.
45. Maltsev AS, Ying J, Bax A (2012) Impact of N-terminal acetylation of α-synuclein on its random coil and lipid binding properties. *Biochemistry* 51(25):5004–5013.
46. Bartels T, Kim NC, Luth ES, Selkoe DJ (2014) N-alpha-acetylation of α-synuclein increases its helical folding propensity, GM1 binding specificity and resistance to aggregation. *PLoS One* 9(7):e103727.
47. Anderson JP, et al. (2006) Phosphorylation of Ser-129 is the dominant pathological modification of α-synuclein in familial and sporadic Lewy body disease. *J Biol Chem* 281(40):29739–29752.
48. Johnson M, Coulton AT, Geeves MA, Mulvihill DP (2010) Targeted amino-terminal acetylation of recombinant proteins in E. coli. *PLoS One* 5(12):e15801–e15805.
49. Zhang X, et al. (1998) Synthesis of squalamine utilizing a readily accessible spermidine equivalent. *J Org Chem* 63(23):8599–8603.
50. Hoyer W, et al. (2002) Dependence of α-synuclein aggregate morphology on solution conditions. *J Mol Biol* 322(2):383–393.
51. Flagmeier P, et al. (2016) Mutations associated with familial Parkinson's disease alter the initiation and amplification steps of α-synuclein aggregation. *Proc Natl Acad Sci USA* 113(37):10328–10333.
52. Brenner S (1974) The genetics of Caenorhabditis elegans. *Genetics* 77(1):71–94.
53. Cohen E, Bieschke J, Perciavalle RM, Kelly JW, Dillin A (2006) Opposing activities protect against age-onset proteotoxicity. *Science* 313(5793):1604–1610.
54. Viswanathan M, Kim SK, Berdichevsky A, Guarente L (2005) A role for SIR-2.1 regulation of ER stress response genes in determining C. elegans life span. *Dev Cell* 9(5):605–615.
55. Lendel C, Bolognesi B, Wahlström A, Dobson CM, Gräslund A (2010) Detergent-like interaction of Congo red with the amyloid β peptide. *Biochemistry* 49(7):1358–1360.

Supporting Information

Perni et al. 10.1073/pnas.1610586114

SI Materials and Methods

Squalamine. Squalamine (as the dilactate salt) was synthesized as previously described (49) and was greater than 97% pure.

Experiments with DOPS:DOPE:DOPC Vesicles.

Protein expression and purification. N-terminally acetylated α-synuclein, which is the most prevalent form of α-synuclein in mammalian cells and also increases membrane affinity (45–47), was obtained as previously described (45). Briefly, N-terminal acetylation of WT α-synuclein was achieved by coexpression of a plasmid carrying the components of the NatB complex with a plasmid containing the wild-type α-synuclein gene, following the protocol described previously (48). We observed that the restrictive conditions of M9 media have a strong effect on the acetylation reaction. Essentially complete acetylation (≥98%) was observed only when using protonated M9 medium, supplemented with 1 g/L protonated IsoGro (Sigma). Unless noted otherwise, all NMR experiments with acetylated α-synuclein were performed on ^{15}N- and ^{13}C-labeled α-synuclein samples, obtained using [^{15}N,^{13}C] IsoGro.

Preparation of vesicles. Phospholipids were purchased from Avanti Polar Lipids as a lyophilized powder of a DOPE/DOPS/DOPC mixture with a 5:3:2 weight ratio (coagulation reagent I). Vesicles were prepared as described previously (27) in 20 mM imidazole buffer [pH 6, 10% (wt/vol)].

NMR spectroscopy. NMR experiments were performed using a 600-MHz Bruker spectrometer equipped with a cryoprobe. The sample temperature was set to 288 K, and the sample buffer composition was 20 mM imidazole, 100 mM NaCl, pH 6. Squalamine is highly soluble in distilled water, but its solubility in 20 mM imidazole, 100 mM NaCl is reduced to ca. 130 μM. Concentrations above this level result in NMR-invisible, light-scattering aggregates. The solubility in PBS (pH 7.4) solution was measured at ca. 35 μM.

CD Spectroscopy. All CD measurements were taken at 20 °C, using a 1-mm path-length cuvette. Samples contained 20 mM Tris (pH 7.4), 100 mM NaCl, 5 μM N-terminally acetylated α-synuclein, and 0.1% wt/vol lipid vesicles (ca. 1.25 mM). The vesicles consisted of 30% DOPS, 50% DOPE, and 20% DOPC.

Experiments with DMPS Vesicles.

Reagents. Sodium salt (DMPS) was purchased from Avanti Polar Lipids. Sodium phosphate monobasic (NaH_2PO_4; BioPerformance certified, ≥99.0%), sodium phosphate dibasic (Na_2HPO_4; ReagentPlus, ≥99.0%), sodium chloride (NaCl; BioXtra, ≥99.5%), and sodium azide (NaN_3; ReagentPlus, ≥99.5%) were purchased from Sigma Aldrich. ThT UltraPure Grade (≥95%) was purchased from Eurogentec.

Protein expression and lipid preparation. WT (nonacetylated) α-synuclein was expressed in *E. coli* and purified as previously described (10, 50). The lipids were dissolved in 20 mM phosphate buffer (NaH_2PO_4/Na_2HPO_4) (pH 6.5), 0.01% NaN_3 and stirred at 45 °C for 2 h. The solution was then frozen and thawed five times, using dry ice and a water bath at 45 °C. The preparation of vesicles was carried out using sonication (Bandelin Sonopuls HD 2070, 3 × 5 min, 50% cycles, 10% maximum power) on ice. After centrifugation, the sizes of the vesicles were checked using dynamic light scattering (Zetasizer Nano ZSP; Malvern Instruments) and were shown to consist of a distribution centered at a diameter of 20 nm.

CD spectroscopy.

Data acquisition. CD samples were prepared as previously described (12) by incubating 20 μM α-synuclein in the presence of 1 mM DMPS vesicles in 20 mM phosphate buffer (pH 6.5), 0.01% NaN_3, and increasing concentrations of squalamine. A squalamine stock solution was prepared by dissolving the molecule in doubly distilled water to a final concentration of 5 mM. Far-UV CD spectra were recorded on a JASCO J-810 instrument equipped with a Peltier thermally controlled cuvette holder at 30 °C. Quartz cuvettes with path lengths of 1 mm were used, and CD spectra were obtained by averaging five individual spectra recorded between 250 nm and 200 nm with a bandwidth of 1 nm, a data pitch of 0.2 nm, a scanning speed of 50 nm/min, and a response time of 1 s. Each value of the CD signal intensity reported at 222 nm corresponds to the average of three measurements, each acquired for 10 s. For each protein sample, the CD signal of the buffer used to solubilize the protein was recorded and subtracted from the CD signal of the protein.

Data analysis. The change in the concentration of α-synuclein bound to the DMPS vesicles with increasing concentration of squalamine was fitted to the same competitive binding model as the one described for the competitive binding of α-synuclein and β-synuclein to DMPS vesicles (22), taking into account the different stoichiometries in which DMPS binds to α-synuclein and squalamine. The equations for the binding equilibria are

$$K_{D,\alpha} = \frac{[DMPS_f]\,[\alpha_f]}{L_\alpha[\alpha_b]} \qquad \text{[S1]}$$

$$K_{D,S} = \frac{[DMPS_f]\,[S_f]}{L_S[S_b]}, \qquad \text{[S2]}$$

where $K_{D,\alpha}$ and $K_{D,S}$ are the binding constants of α-synuclein and squalamine, respectively; $[\alpha_f]$ and $[\alpha_b]$ are the concentrations of free and bound α-synuclein; $[S_f]$ and $[S_b]$ are the concentrations of free and bound squalamine; $[DMPS_f]$ is the concentration of free DMPS; and L_α and L_S denote the stoichiometries in which DMPS binds to α-synuclein and squalamine, i.e., the number of molecule of DMPS interacting with one molecule of either α-synuclein or squalamine, respectively.

By using the mass conservation equations,

$$[\alpha] = [\alpha_b] + [\alpha_f] \qquad \text{[S3]}$$

$$[S] = [S_b] + [S_f] \qquad \text{[S4]}$$

$$[DMPS] = [DMPS_f] + L_S[S_b] + L_\alpha[\alpha_b], \qquad \text{[S5]}$$

where $[\alpha]$, $[S]$, and $[DMPS]$ are the total concentrations of α-synuclein, squalamine, and DMPS, respectively. An expression for $[\alpha_b]$ in terms of $K_{D,\alpha}$, $K_{D,S}$, L_α, L_S, $[\alpha]$, $[S]$, and $[DMPS]$ can be derived. This is the standard solution of the cubic equation:

$$K_{D,\alpha} = \frac{([DMPS] - L_S[S_b] - L_\alpha[\alpha_b])([\alpha] - [\alpha_b])}{L_\alpha[\alpha_b]} \qquad \text{[S6]}$$

$$[S_b] = \frac{[DMPS] - L_\alpha[\alpha_b] + K_{D,S}L_S + L_S[S]}{2L_S} - \frac{\sqrt{4L_S([\alpha_b]L_\alpha[S] - [DMPS][S]) + \left([DMPS] - [\alpha_b]L_\alpha + K_{D,S}L_S + L_S[S]\right)^2}}{2L_S}. \quad \textbf{[S7]}$$

Its solution is not shown here due to its length. For each data point, the concentrations $[\alpha_b]$, $[S]$, and $[DMPS]$ are known, and the equilibrium constant and stoichiometry for the α-synuclein/DMPS system, $K_{D,\alpha}$ and L_α, were set to the values determined previously (12). The variation of $[\alpha_b]$ at a fixed [DMPS] (1 mM) and $[\alpha]$ (20 μM), with increasing $[S]$, was fitted using the resulting equation with two unknowns, $K_{D,S}$ and L_S, and the best fit is obtained for $K_{D,S} = 67$ nM and $L_S = 7.4$ (Fig. 3*B*).

Aggregation kinetics.

Sample preparation and data acquisition. α-Synuclein was incubated in 20 mM sodium phosphate (pH 6.5), 0.01% NaN_3, in the presence of 50 μM ultrapure ThT, 100 μM DMPS vesicles, and increasing concentrations of squalamine (0–10 μM). The stock solution of squalamine was prepared by dissolving the molecule in 20 mM phosphate buffer to a final concentration of 100 μM. The change in the ThT fluorescence signal with time was monitored using a plate reader (BMG Labtech) under quiescent conditions at 30 °C. Corning 96-well plates with half-area (black/clear bottom polystyrene) nonbinding surfaces were used for each experiment. The data were then analyzed as described previously (12).

Data analysis. To determine the rate of lipid-induced aggregation of α-synuclein at different squalamine concentrations, we used the same model as the one describing the inhibition of α-synuclein lipid-induced aggregation by β-synuclein (22): The rate depends on the fractional coverage of a lipid vesicle in α-synuclein ($\theta\alpha$) and we define n_b as the reaction order with respect to $\theta\alpha$. We can adapt the equations given in ref. 12 to reflect this,

$$M(t) = \frac{K_M k_+ m(0)^{n+1} k_n [DMPS]\theta_\alpha^{n_b} t^2}{2(K_M + m(0))L_\alpha} \quad \textbf{[S8]}$$

where t is the time, $M(t)$ is the aggregate mass, $m(0)$ is the free monomer concentration, K_M is the saturation constant of the elongation process, k_n and k_+ are the rate constants of nucleation and elongation, respectively, and $\frac{[DMPS]}{L_\alpha}$ is the concentration of protein-binding sites at the surface of the membrane. We initially used Eq. S8 to fit the early times of the kinetic traces measured for α-synuclein in the presence of 100 μM DMPS and in the absence of squalamine (where $\theta_\alpha = 1$ as we are in a regime where the vesicles are saturated), with K_M, $k_n k_+$, and n being global fitting parameters (fit, Fig. 3*B*). The global fit yields $n = 0.624$, $K_M = 54$ μM, and $k_n k_+ = 9.9 \times 10^{-3}$ $M^{-(n+1)}$ s^{-2}. The values obtained for these three parameters were then used as inputs into the fitting of the data in the presence of squalamine. The assumption that the presence of squalamine merely alters the fraction of α-synuclein bound but does not affect any of the other rates is implicit. We then fitted the data in the presence of squalamine, with all parameters fixed to their values in the absence of squalamine, with the exception of $\theta_\alpha^{n_b}$. All fits were within error of the experimental data. This way we obtain $\theta_\alpha^{n_b}$ at all α-synuclein and squalamine concentrations.

We then used a simplified competitive binding model to analyze the change of $\theta_\alpha^{n_b}$ with changing squalamine:α-synuclein ratios, to determine n_b. In the competitive binding model described above, the solution to Eq. S6 simplifies when all binding sites on the vesicles can be assumed to be occupied, as is the case in the kinetic experiments. In this case Eq. S5 becomes $[DMPS] \approx L_S[S_b] + L_\alpha[\alpha_b]$. The concentration of bound α-synuclein is then simply given by

$$[\alpha_b] = \frac{[DMPS]L_\alpha\kappa - [DMPS]L_S - [\alpha]L_\alpha L_S - L_\alpha L_S[S]\kappa}{2(L_\alpha^2\kappa - L_\alpha L_S)} + \frac{\sqrt{4[\alpha][DMPS]L_S(L_\alpha^2\kappa - L_\alpha L_S) + \left(\begin{array}{c}[DMPS]L_S + [\alpha]L_\alpha L_S - \\ [DMPS]L_\alpha\kappa + L_\alpha L_S[S]\kappa\end{array}\right)^2}}{2(L_\alpha^2\kappa - L_\alpha L_S)}, \quad \textbf{[S9]}$$

where $\kappa = \frac{K_{D,\alpha}}{K_{D,S}}$. The global fits of $\theta_\alpha^{n_b} = \left(\frac{[\alpha_b]L_\alpha}{[DMPS]}\right)^{n_b}$ agree well with the data (Fig. 3*D*) and we obtain $n_b = 5.5$.

Mass Spectrometry Experiments on α-Synuclein and Aβ Fibrils.

Preparation of fibrils. α-Synuclein fibrils were prepared as described previously (10, 51). Briefly, a 500-μL sample of α-synuclein at a concentration of 600 μM was incubated in 20 mM phosphate buffer (pH 6.5) for 72 h at about 40 °C and stirred at 1,500 rpm with a Teflon bar on an RCT Basic Heat Plate (IKA). Fibrils were diluted to a monomer equivalent concentration of 200 μM, divided into aliquots, flash frozen in liquid N_2, and stored at −80 °C for experiments. For experiments with the Aβ peptide (in this work we used the 42-residue form), fibrils were prepared as described previously (13). Briefly, Aβ monomer at a concentration of 78 μL was incubated in 20 mM phosphate buffer (pH 8) with 200 μM EDTA, 0.02% NaN_3, for 6 h at about 37 °C. Before mass spectrometry analysis, 78 μM of equivalent α-synuclein and Aβ fibrils was centrifuged at 100,000 × *g* for 1 h at the ultracentrifuge. The pellet was then resuspended in the same volume of Tris buffer for further analysis.

Preparation of samples for mass spectrometry experiments. Fibrils of α-synuclein or Aβ at a concentration of 10 μM were incubated with 10 μM squalamine in 20 mM Tris (pH 7.4), 100 mM NaCl overnight under quiescent conditions at room temperature. The samples were afterward centrifuged at 100,000 × *g* for 30 min at the ultracentrifuge. The supernatant was then removed for analysis. In the present work the experiments were run using a Waters Corporation Xevo G2-S QTOF.

Experiments on Human SH-SY5Y Neuroblastoma Cells.

Preparation of oligomers. Samples enriched in oligomeric α-synuclein species were prepared as previously described (34). Briefly, monomeric α-synuclein was lyophilized in Milli-Q water and subsequently resuspended in PBS, pH 7.4, to give a final concentration of ca. 800 μM (12 mg/mL). The resulting solution was passed through a 0.22-μm cutoff filter before incubation at 37 °C for 20–24 h under quiescent conditions. Very small amounts of fibrillar species formed during this time were removed by ultracentrifugation for 1 h at 90,000 rpm (using a TLA-120.2 Beckman rotor, 288,000 × *g*). The excess monomeric protein and some small oligomers were then removed by multiple filtration steps, using 100-kDa cutoff membranes. The final concentration of oligomers was estimated based on the absorbance at 275 nm, using a molar extinction coefficient of 5,600 $M^{-1}{\cdot}cm^{-1}$.

Neuroblastoma cell culture. Human SH-SY5Y neuroblastoma cells (A.T.C.C.) were cultured in DMEM, F-12 HAM with 25 mM Hepes and $NaHCO_3$ (1:1) and supplemented with 10% FBS, 1 mM glutamine, and 1.0% antibiotics. Cell cultures were maintained in a 5% CO_2 humidified atmosphere at 37 °C and grown until they reached 80% confluence for a maximum of 20 passages (24).

MTT reduction assay. α-Synuclein oligomers (24) (0.3 μM) were incubated with or without increasing concentrations (0.03 μM,

0.1 μM, 0.3 μM, 1 μM, and 3 μM) of squalamine for 1 h at 37 °C under shaking conditions and then added to the cell culture medium of SH-SY5Y cells seeded in 96-well plates for 24 h. The protein:squalamine molar ratios used here were 10:1, 3:1, 1:1, 1:3, and 1:10. The MTT reduction assay was performed as previously described (43).

Measurement of intracellular ROS. α-Synuclein oligomers (0.3 μM) were preincubated for 1 h with or without increasing concentrations (0.03 μM, 0.3 μM, and 3 μM) of squalamine for 1 h at 37 °C under shaking and then added to the cell culture medium of SH-SY5Y cells seeded on glass coverslips for 15 min. To detect intracellular ROS production, cells were then loaded with 10 μM CM-H_2DCFDA (Life Technologies) as previously described (43). Cell fluorescence was analyzed by a TCS SP5 scanning confocal microscopy system (Leica Microsystems) equipped with an argon laser source, using the 488-nm excitation line. A series of 1.0-μm-thick optical sections (1,024 × 1,024 pixels) was taken through the cells for each sample, using a Leica Plan Apo 63 oil immersion objective, and then projected as a single composite image by superimposition. The confocal microscope was set at optimal acquisition conditions, e.g., pinhole diameters, detector gain, and laser powers. Settings were maintained constant for each analysis.

Oligomer binding to the cellular membrane. SH-SY5Y cells were seeded on glass coverslips and treated for 15 min with α-synuclein oligomers (0.3 μM) and increasing concentrations (0.03 μM, 0.1 μM, 0.3 μM, 1 μM, and 3 μM) of squalamine. After incubation, the cells were washed with PBS and counterstained with 5.0 μg/mL Alexa Fluor 633-conjugated wheat-germ agglutinin (Life Technologies). After washing with PBS, the presence of oligomers was detected with 1:250 diluted rabbit polyclonal anti–α-synuclein antibodies (Abcam) and subsequently with 1:1,000 diluted Alexa Fluor 488-conjugated anti-rabbit secondary antibodies (Life Technologies). Fluorescence emission was detected after double excitation at 488 nm and 633 nm by the scanning confocal microscopy system described above and three apical sections were projected as a single composite image by superimposition.

C. elegans Experiments.

Media. Standard conditions were used for the propagation of *C. elegans* (52). Briefly, the animals were synchronized by hypochlorite bleaching, hatched overnight in M9 (3 g/L KH_2PO_4, 6 g/L Na_2HPO_4, 5 g/L NaCl, 1 M $MgSO_4$) buffer, and subsequently cultured at 20 °C on nematode growth medium (NGM) [1 mM $CaCl_2$, 1 mM $MgSO_4$, 5 μg/mL cholesterol, 250 M KH_2PO_4 (pH 6), 17 g/L Agar, 3 g/L NaCl, 7.5 g/L casein] plates seeded with the *E. coli* strain OP50. Saturated cultures of OP50 were grown by inoculating 50 mL of LB medium (10 g/L tryptone, 10 g/L NaCl, 5 g/L yeast extract) with OP50 and incubating the culture for 16 h at 37 °C. NGM plates were seeded with bacteria by adding 350 μL of saturated OP50 to each plate and leaving the plates at 20 °C for 2–3 d. On day 3 after synchronization, the animals were placed on NGM plates containing 5-fluoro-2′ deoxy-uridine (FUDR) (75 μM, unless stated otherwise) to inhibit the growth of offspring.

Strains. The following strains were used. zgIs15 [P(unc-54):: αsyn:: YFP]IV (OW40): In OW40, α-synuclein fused to YFP relocates to inclusions, which are visible as early as day 2 after hatching and increase in number and size during the aging of the animals, up to late adulthood (day 17) (25). rmIs126 [P(unc-54)Q0::YFP]V (OW450): In OW450, YFP alone is expressed and remains diffusely localized throughout aging (25). dvIs2 [pCL12(unc-54/ human Aβ 1–42 peptide minigene) + pRF4]: Where $A\beta_{42}$ aggregates giving rise to adult onset paralysis and egg-laying, deficiency is observed when the temperature is raised to 20 °C.

Squalamine administration. Aliquots of NGM media containing FUDR (75 μM) were autoclaved, poured, seeded with 350 μL OP50 culture, and grown overnight. After incubating for up to 3 d at room temperature, 2.2-mL aliquots of squalamine dissolved in water at different concentrations were spotted atop the NGM plates. The plates were then placed in a sterile laminar flow hood at room temperature to dry. We first observed that the compound was toxic when administered to the worms from L1 larval stage (25% worm death), probably due to the high membrane permeability of the worms in this stage. For the final experiments, worms were transferred onto the squalamine-seeded plates directly at larval stage L4 and they were exposed to squalamine for the whole duration of the experiment.

Thrashing assays. At different ages, animals were placed in a drop of M9 buffer and allowed to recover for 30 s (to avoid observing behavior associated with stress) after which the number of body bends was counted for either 30 s or 1 min. For blinded motility assays, adult animals were randomly picked from the treated and untreated populations and measured for motility without knowledge of the squalamine concentration. Thirty animals were counted in each experiment unless stated otherwise. Experiments were carried out in triplicate and the data from one representative experiment are shown in Fig. S4. Statistical analysis was performed using Graphpad Prism software (GraphPad Software) (37).

Automated motility assay. All *C. elegans* populations were cultured at 20 °C and developmentally synchronized from a 4-h egg lay. At 64–72 h post-egg lay (time 0) individuals were transferred to FUDR plates or into multiwells and body movements were assessed over the times indicated. For experiments carried out on agar plates, at different ages, the animals were washed off the plates with M9 buffer and spread over an OP50 unseeded 6-cm plate, after which their movements were recorded at 30 fps, using a novel microscopic setup for 30 s or 1 min. For screenings in multiwells, worms were mixed on a bench-top plate shaker at 700 rpm for 7 min to evenly distribute sedimented OP50 and induce full worm motility. Immediately after shaking, worms were staged on the platform for imaging. File collection was initiated 60 s after shaking. Up to 200 animals were counted in each experiment unless stated otherwise. One experiment that is representative of the three measured is shown in Fig. 5. Movies were analyzed using a custom-made tracking code.

Paralysis assays. Paralysis assays were performed by transferring L4 larvae synchronized animals to NGM plates and they were grown at 15 °C until the first day of adulthood (2 d after L4) to avoid developmental defects of the vulva. The L4 larvae or the young adult animals were transferred to squalamine plates containing FUDR and the temperature was raised to 20 °C. Each individual experiment was initiated with 100 L4 or young adult animals per strain. The animals were tested for paralysis by tapping their noses and tails, prodding with a platinum wire as described previously (53) every day for 14 consecutive days. Worms that moved their noses but failed to move their bodies were scored as paralyzed. Data from one representative of three experiments are shown in Fig. S5. Analysis was performed using Graphpad Prism software (GraphPad Software) (37).

Quantification of inclusions. To monitor the number of inclusions in each worm, individual animals were mounted on 2% agarose pads, containing 40 mM NaN_3 as an anesthetic, on glass microscope slides for imaging. For quantification of the number of inclusions in α-synuclein:YFP animals, only the frontal region of the worms was considered (25). The number of inclusions in each animal was quantified using a Leica MZ16 FA fluorescence dissection stereomicroscope (Leica Microsystems) at a nominal magnification of 20× or 40×, and images were acquired using an Evolve512 Delta EMCCD camera, with high quantum efficiency (Photometrics). Measurements on inclusions were performed using ImageJ software (54) (National Institutes of Health). At least 50 animals were examined per condition, unless stated otherwise. All experiments were carried out in triplicate and the data from one representative experiment are shown in Figs. 4

and 5. Student's *t* test was used to calculate *P* values, and all tests were two-tailed unpaired unless otherwise stated.

Western blot analysis. For comparison of α-synuclein levels, ca. 3,000 adults were collected in S-basal (52) in triplicate and then frozen in liquid N_2. Samples were then extracted in Urea/SDS buffer (8 M urea, 2% SDS, 50 mM Tris, 1× proteinase inhibitors) (Roche Holding) and disrupted via sonication. Samples at the appropriate concentration were added to NuPAGE LDS Sample Buffer (1×) and NuPAGE Sample Reducing Agent (1×) (Life Technologies) and heated at 70 °C for 10 min. The material was resolved via NuPAGE Novex 4–12% Bis-Tris Protein Gels (Life Technologies) and then transferred to nitrocellulose membranes, using an iBlot Dry Blotting System (Life Technologies), and blocked overnight at 4 °C in 5% BSA. Membranes were then probed at room temperature with SYN-1 anti–α-synuclein antibody, clone 42 (BD Biosciences) 1:500. Anti–α-tubulin, clone B-5-1-2 (Sigma-Aldrich) 1:10,000, was used to standardize total protein loading. An Alexa 488-conjugated secondary antibody, A11029 (Life Technologies), was used for detection.

SI Text

Automated Motility Assay. We built a simple, robust, compact, cost-effective and high-throughput setup to track *C. elegans* during swimming and crawling. An LED backlight illuminator with long life span and flicker-free and shadow-free illumination was used to illuminate worms moving in M9 buffer on a thin agar plate or in multiwells. The swimming worms were visualized by using a high-performance imaging lens and a machine vision camera. The movies of the swimming worms were taken at a high number of fps for 30 s or 1 min. Different fields of view were obtained simply by changing the distance between the sample and the lens, for a fixed focal length of the lens and camera sensor size. Using this setup we were able to image successfully at the same time up to 200 swimming animals over the whole surface of a 6-cm agar plate or inside multiwells.

To analyze the worm movement from the movies, the first step was to detect and subtract the background. If all worms are alive, this procedure can be carried out by temporally averaging the movies. If some of the worms are dead, however, this method will skew the final statistics because the dead worms will be taken as part of the background and thus not be included in the signal. This is particularly important for high-throughput testing of drugs, because certain drugs might influence the life-to-death ratio and paralysis rate. Thus, the background must be estimated without using temporal information. In our method we begin by defining a Gaussian adaptive threshold of the image in such a way that all worms are identified. Such a threshold that ensures detection of all worms will also incorrectly elaborate some of the background signal as worms and so is not a completely reliable detection mechanism in itself. All pixels marked as worms are then recalculated by interpolating from pixels not marked as worms. This procedure avoids removing the dead worms as part of the background. The method requires the movie to be quite regular, however, and hence other items, such as the edge of a Petri dish, must first be masked by other methods. After background subtraction a second (nonadaptive) thresholding procedure is performed. Morphological operations are next used to remove speckles (morphological opening) and to close holes that can appear in the worms after the thresholding (morphological closing). We label all separated regions of the thresholded image and remove all regions that have an area too small or big to be a single worm. The remaining labeled regions are identified as individual worms. The positions of said regions are then stored for each frame. Subsequently these regions are linked across the frames by standard tracking algorithms, even taking into account a worm disappearing or overlapping in a few frames. The eccentricity, a measure of the ratio of the minor and major ellipse axes, of each tracked worm can then be used to estimate the worm bending as a function of time.

Detection of the Interaction of Squalamine with Monomeric α-Synuclein at High Concentrations in the Absence of Lipids. The changes in the NMR spectrum indicate that the α-synuclein–squalamine interaction is in the fast exchange regime, as the residues of α-synuclein that are affected by the binding progressively shift their resonance positions as the concentration of squalamine is increased; as a consequence of the broadening a loss of intensity is also observed (Fig. S1). An indication that the interaction involves an aggregated state of squalamine comes from the observation that at a high squalamine concentration some of the C-terminal residues of α-synuclein (e.g., Y136) experience a large degree of line broadening despite showing only modest changes in chemical shifts. Resonance broadening is likely to result from two factors: a chemical exchange contribution, caused by perturbations in chemical shifts, and an increase in the dipolar contribution to the transverse relaxation rate, R2, caused by the increased size of the complex. Considering that the chemical shift change for Y136 is small, the R2 contribution must dominate, suggesting that the complex is significantly larger in size than the monomer. This finding is consistent with the involvement of multimeric squalamine in the interaction, analogous to the interaction between α-synuclein and micellar Congo Red (CR) (55).

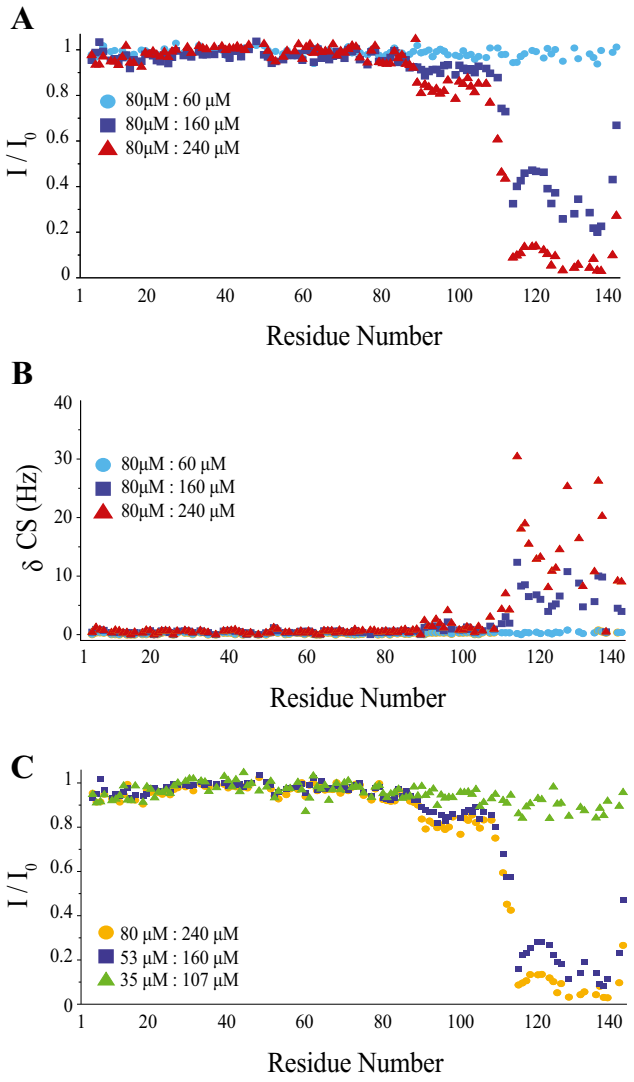

Fig. S1. Squalamine interacts directly with α-synuclein at high concentrations. (*A*) Ratios of α-synuclein HSQC peak heights in the presence of different concentrations of squalamine compared with free α-synuclein. The sample contained 80 μM α-synuclein, and three concentrations of squalamine were tested: 60 μM (blue circles), 160 μM (violet squares), and 240 μM (red triangles). The buffer conditions were 20 mM imidazole (pH 6), 100 mM NaCl. (*B*) Changes in chemical shifts measured at a frequency of 600 MHz 1H resulting from squalamine addition compared with free α-synuclein. δ_{CS} was defined as $\delta_{CS} = \sqrt{\delta_{CS} + \left(\frac{\delta_H}{2}\right)^2}$, where δ_N and δ_H are the changes in resonance frequency (in hertz units) for ^{15}N and ^{1}H, respectively. The sample contained 80 μM α-synuclein, and three concentrations of squalamine were tested: 80 μM (blue circles), 160 μM (violet squares), and 240 μM (red triangles). (*C*) Ratios of α-synuclein HSQC peak heights are shown for three samples at different concentrations with a fixed squalamine:α-synuclein ratio: 80 μM α-synuclein and 240 μM squalamine (yellow circles), 53 μM α-synuclein and 160 μM squalamine (dark blue squares), and 35 μM α-synuclein and 107 μM squalamine (green triangles).

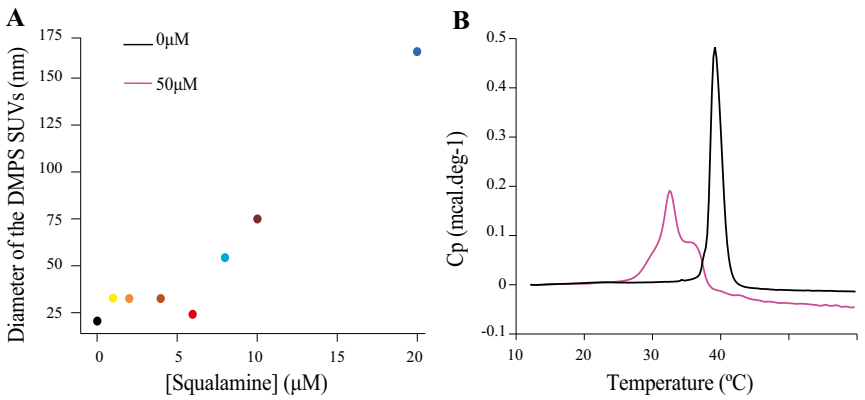

Fig. S2. Effect of squalamine on the size and the thermotropic properties of DMPS vesicles. (*A*) Change in the diameter of DMPS vesicles (100 μM) with increasing concentrations of squalamine measured by dynamic light scattering. (*B*) Differential scanning calorimetry trace of 500 μM DMPS in the absence and presence of 50 μM squalamine.

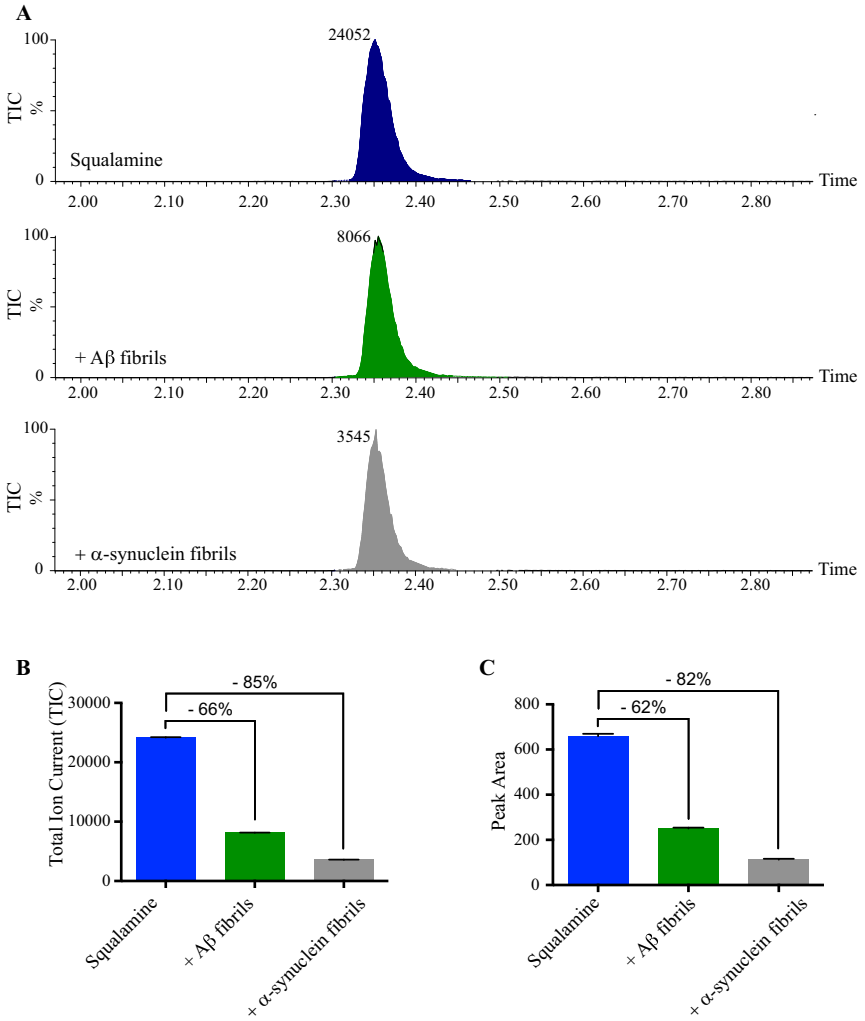

Fig. S3. Squalamine binding to Aβ and α-synuclein fibrils. (*A*) Total ion current (TIC) of 10 μM squalamine (*Top*), TIC corresponding to the supernatant fraction after incubation with Aβ (*Middle*), and α-synuclein fibrils (*Bottom*), respectively. Experiments were carried out in triplicate and one representative experiment is shown. (*B*) TIC averaged over three independent experiments. (*C*) Peak area averaged over three independent experiments. α-Synuclein and Aβ fibrils were obtained as previously described (10, 13) and incubated overnight with 10 μM squalamine.

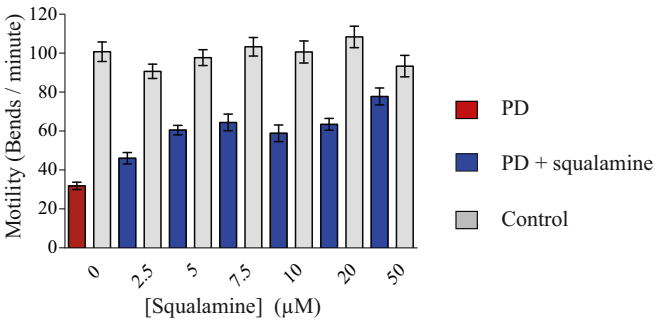

Fig. S4. Squalamine recovers the severe muscle paralysis associated with overexpression of α-synuclein in PD worms (25). For experiments carried out in solid media, the protective effect is maximal at day 4 for 50 μM squalamine. Red bars, PD; blue bars, treated PD; gray bars, controls. The plots show one representative of three experiments. Error bars represent the SEM.

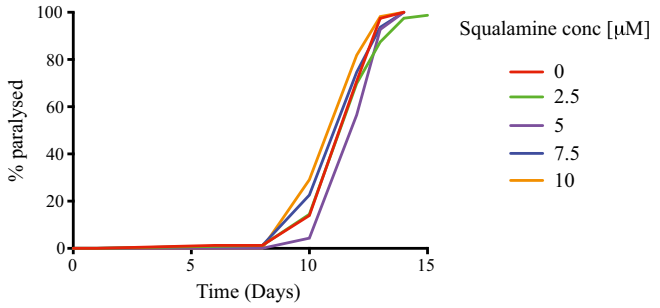

Fig. S5. Exposure to squalamine has less relevant effects on an Aβ worm model. Squalamine administration at a concentration of 1–10 μM had no significant protective effect (e.g., no decrease in the time of the onset of the paralysis) for an Aβ worm model CL2006 (40). The plots show one representative of three experiments.

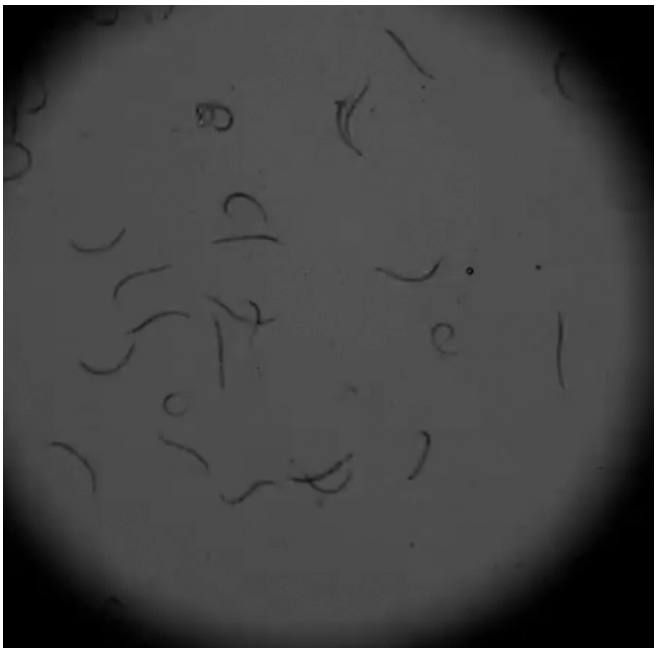

Movie S1. The mobility of untreated control worms at day 4 of adulthood.

Movie S1

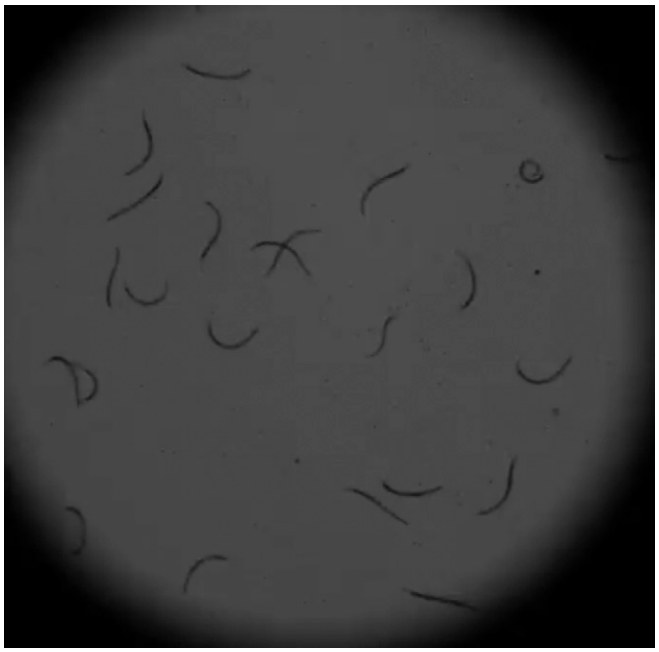

Movie S2. The mobility of control worms treated with 50 μM squalamine at day 4 of adulthood. Squalamine does not notably affect the motility of control worms.

Movie S2

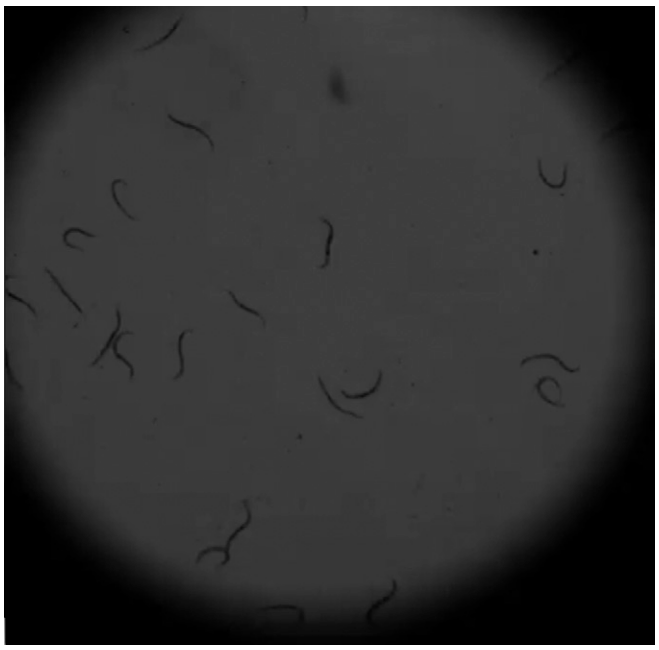

Movie S3. The mobility of untreated PD worms at day 4 of adulthood. It is clear the motility dysfunction is induced by α-synuclein overexpression.

Movie S3

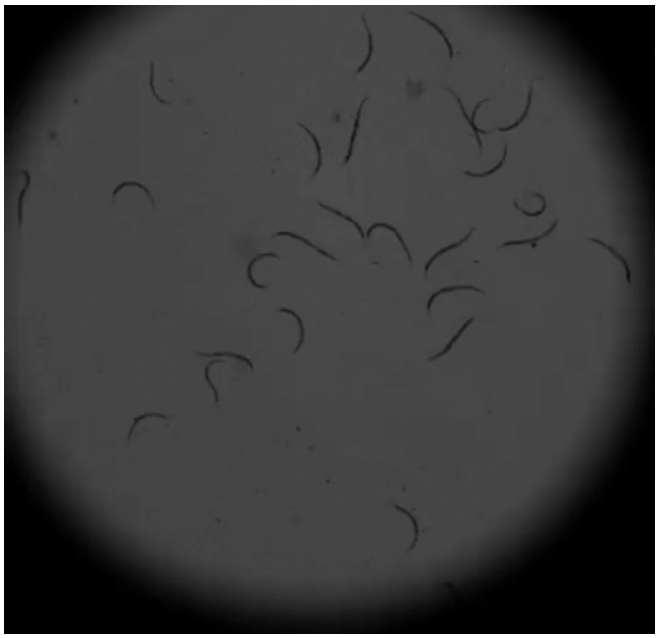

Movie S4. The mobility of treated PD worms at day 4 of adulthood. Squalamine greatly rescues the motility dysfunction induced by α-synuclein overexpression.

Movie S4